A numerical study of simulations of an ultrasonic waveguide experiment for Power-law fluids.

Eva Benschop

to obtain the degree Bachelor of Science
at Delft University of Technology,
to be defended publicly on July 12th 2022

Student number: 5132118

Project duration: April 18th, 2022 - July 12th, 2022

Thesis committee: Dr. ir. Martin Rohde, TU Delft, supervisor
Prof. Dr. ir. Jan Leen Kloosterman, TU Delft

Highlights

•A simulation of an ultrasonic waveguide amplitude experiment was developed. When simulating, the velocity profile, the shear-stress and the amplitude should be calculated for every height.

•There is a noticeable difference in amplitude attenuation for step sizes, in the height, $\Delta z = \lambda$ and $\Delta z = \lambda/8$. The used initial amplitude has influence on the retrieved rheology.

•The results show that is informative to perform the simulation with parameters that are realistic for the physical set-up.

Abstract

To comply with safety regulations it is important to simulate extreme situations in the MSFR. To develop these simulations more should be known about the rheology of the molten salt. This can be achieved by using an ultrasonic waveguide viscometer. The viscometer works by sending a shear wave down a thin metal plate and measuring the amplitude attenuation, which is in direct relation with the viscosity. The measurements can be done for Newtonian fluids as the velocity profile is known, but for Power-law fluids a relation between the amplitude and rheology should be found. To find this relation it is helpful to use a simulation of the measurements.

In this thesis a numerical model for the ultrasonic waveguide amplitude measurement was made. The simulation was based on a previous simulation, in which an assumption was made to reduce computation time. The assumption was that $\tau_{yx,0}$ scaled with $B(z)^m$. By using the assumption it was no longer needed to calculate the rheology for every z. In this thesis the validity of this assumption was investigated. By rewriting the code, without using the assumption, the validity could be checked. If the assumption made in the previous version of the code was valid, a linear relation would show when $\tau_{yx,0}$ was plotted against $B(z)^m$.

The code was benchmarked with water. An exponential decay of the amplitude against the height was observed as expected. The influence of the step size in the height, Δz, was investigated. This was done by plotting the amplitude attenuation and velocity profile for different step sizes: $\Delta z = \lambda$, $\Delta z = \lambda/2$, $\Delta z = \lambda/4$ and $\Delta z = \lambda/8$. A difference could be seen in the amplitude attenuation, but no difference could be seen in the velocity profile.

For three Power-law fluids the amplitude attenuation was plotted, $\dot{\gamma}$ against τ_{yx} and $\tau_{yx,0}$ was plotted against $B(z)^m$. For soybean oil and ethylene glycol it was observed that the relation between $\tau_{yx,0}$ and $B(z)^m$ was not a linear one. When $\tau_{yx,0}$ was plotted against $B(z)^m$ for ketchup a plot was produced in which the simulation data points where scattered. This could be a numerical instability so the simulation was repeated with step sizes $\Delta z = \frac{\lambda}{4}$ and $\Delta z = \frac{\lambda}{20}$. This did not reduce the scattering and thus the results of ketchup could not be taken into account for the conclusion. The source of the numerical instability should be investigated further. The $\tau_{yx,0}$ against $B(z)^m$ plot was made for one more fluid, blood. The relation in this plot was the best approximation of a linear relation. When the amplitude attenuation was compared it was discovered that the slope was different for the two versions of the code. The values found from the simulation of m where less accurate than with the previous version, however, the values of K_m were much more accurate. The value of K_m found for ethylene glycol was not physical, as it was negative. Other ways of determining m and K_m should be investigated. It should be investigated if the results improves if a larger z range is simulated.

It can be concluded that the assumption made in the previous version of the code is not valid. As the relations found where close to linear, it should be investigated how much difference the two codes make when retrieving m and K_m with other methods. The computation time is increased significantly, it could be investigated if this can be reduced. The effect of the initial amplitude should be investigated. Lastly, the simulation can be extended to Bingham and Casson fluids.

Contents

1. Introduction

There is an increasing need for new sustainable ways to generate electricity due to the climate crisis. A swift transition to more sustainable energy sources is desirable at this point in time. A promising new of sustainable energy sources are nuclear reactors. Nuclear reactors must comply with strict safety measures. One new type of reactors is the molten salt reactor (MSFR). Before the reactor can be taken into use it must comply with all these strict regulations. To achieve this many simulations must be performed to research what happens in extreme situations and to optimize the performance of the reactor. Therefore more about the properties of this reactor should be known to develop these simulations.

1.1. Molten salt fast reactor

The molten salt reactor is a type of nuclear reactor that has been around since the 1960's. This type of reactor was operating for several years. With research coming to a halt around 1975 [1]. In this type of reactor the fuel is dissolved in a liquid salt that also acts as a coolant [1]. In light of the energy crisis interest in this concept has risen in popularity again due to its sustainability, optimal waste control and nuclear safety characteristics [2]. The molten salt fast reactor (MSFR) is the only fourth generation reactor with a liquid salt to carry the fuel. A schematic of a MSFR is shown in Figure 1.1.

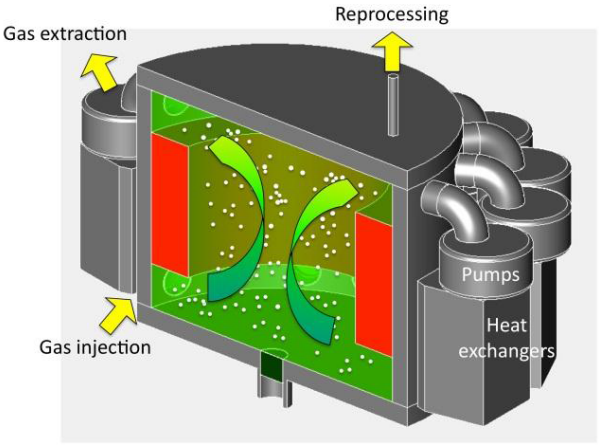

Figure 1.1.: A schematic view of a MSFR core [2]

The salt contains of a mixture of lithium fluoride and with dissolved low enriched uranium and thorium [3]. The reactor operates at high temperatures of around 750 ° C. One of the innovative safety measures of the MSFR is the freeze plug. When the reactor is overheating or there is a loss of power, a plug at the bottom of the reservoir melts. The fluid then is drained in tanks where it is safely stored below the reactor core [2].

As mentioned before, nuclear reactors have strict safety guidelines to comply with. SAMOSAFER [2] is a project funded by the European Commision that develops numerical models. These models are used to learn more about the safety of the MSFR and to search for ways to limit waste. Extreme accidents can be simulated to explore how the reactor will behave in these situations. It is expected that the MSFR complies with all regulations in 30 year time [2]. It is important to know the behavior and properties of such a reactor to comply with safety rules and to preform the necessary simulations. One of these properties is the rheology of the molten salt. To know more about the rheology a viscosity measurement is important to preform. Because of the extreme circumstances under which the reactor operates, such as the high temperature and corrosivity of the fluid, many viscometers are not suited for this kind of measurement. Moreover the measurement should be done remotely due to the radioactivity of the fluid. A possible suitable viscometer is the ultra sonic viscometer. In this thesis this viscometer will be investigated.

1.2. Ultrasonic viscometer

The idea of using ultrasonic waves to determine rheology was first proposed by Manson [4]. The original proposal was to send a sound wave directly through the fluid. When the wave reflects and the amplitude is measured again it is attenuated, the wave has lost energy. Manson states that this loss of energy can be used to determine rheological properties. However the corrosivity of the molten salt is too extreme for the transducer and thus another solution is needed.

In further research done by Vogt the use of a waveguide is explored [5]. This is often a metal object in which shear waves propagate, in the research performed by Vogt it was a partiality immersed cylindrical waveguide. The waveguide can differ in shape and material. The wave is generated by a transducer that sits on top of the wave guide which does not touch the fluid. This is useful because when a material reaches it's curie temperature it is not longer able to send or receive ultrasonic signals [6]. By using a waveguide the transducer will not reach this temperature and the corrosivity of the molten salt does not longer damage the transducer.

Cegla [6] researched non destructive measurements in harsh environments. He describes that only one mode of shear waves can exist in the wave guide for a certain frequency thickness product range [6]. Therefore the frequency and size of the wave guide should be taken into account while making the experimental setup. In this research a rectangular thin wave guide will be used as shown in Figure 1.2

This viscometer is tested and gives reasonable results for Newtonian fluids [8]. It does not yet work for non-Newtonian fluids. The reason is that Newtonian fluids have an analytical solution for the velocity profile. The viscosity can be found directly from the amplitude attenuation. However the molten salt is expected to be a non-Newtonian fluid. Non-Newtonian fluids have a more complex rheology. Therefore it is not immediately possible to retrieve the rheology from the amplitude attenuation. Assumptions have to be made to simplify the problem. Rohde [7] derived an analytical model for power law fluids, a type of non-Newtonian fluids. This can be used to retrieve the rheology from the measurements. This analytical model will be used in this thesis.

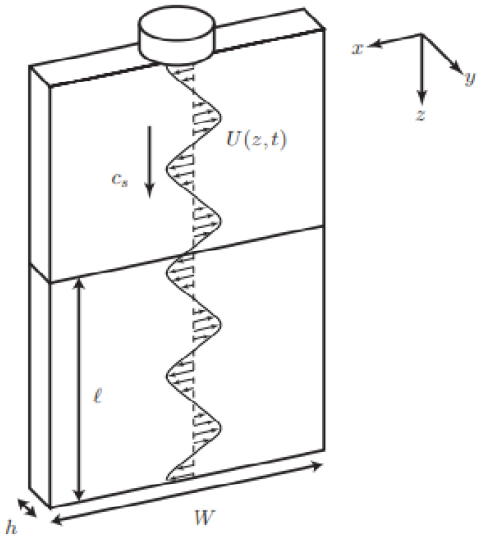

Figure 1.2.: The wave guide set-up. With c_s the propagation velocity in the z direction $[ms^{-1}]$, l the length in the z direction $[m]$, W the width in the x direction $[m]$, h the thickness in the y direction $[m]$ and $U(z,t)$ the form of the generated shear wave by the transducer. [7]

1.3. Previous research at TU Delft

This set-up is previously researched by Rook [8] for Newtonian fluids. Rook managed to measure the viscosity for low viscosity Newtonian fluids [8]. This was done by using the analytical solution for the velocity profile of Newtonian fluids. Such an analytical solution does not exists for power-law fluids. Therefore Rohde [7] proposed an analytical model and method to retrieve the rheology based on the research of Ai and Vafai [9]. In this method a linear fit is used to retrieve the rheology. Borstlap [10] made a numerical simulation of the wave guide measurement for Newtonian and power law fluids. This was used to explore the solution Rohde proposed. This did not yet resulted in values close to the literature. Schuringa [11] studied several other solutions to retrieve rheological properties also using numerical simulations based on the simulation made by Borstlap. This resulted is slightly better results but not yet close enough to the literature values. Van Dijk followed with a different approach [12]. She used dimension analysis and tried to fit the found relation using the earlier named numerical model made by Borstlap and adjusted by Schuringa. This still gave results that differed too much from the literature value.

1.4. Thesis outline

To understand the behavior of the fluid in the MSFR it is important to know the rheology of the molten salt. To improve the understanding about the rheology it is desirable to be able to retrieve the rheological properties of a Power-law fluid from the waveguide amplitude measurements. This leads to the following general research question:

•How can the rheological properties of Power-law fluids be accurately retrieved from the am-

plitude measurements in the ultrasonic waveguide viscometer?

Because of the complexity of the Power-law fluid rheology a relation should be found between the amplitude of the shear wave in the waveguide and the rheological properties. To achieve this it is useful to simulate the experiment. By simulating the experiment no noise is present making it easier to find the best relation. The goal of this thesis is to deliver a numerical simulation of the ultrasonic waveguide amplitude measurments that can be used to find a relation between the amplitude of the shear-wave and the rheology of Power-law fluids.

A possibility is that in the numerical model used in most of the previous research an assumption is made, which is not completely correct and should be checked. The assumption was that $\tau_{yx,0}$ scales linearly with $B(z)^m$. This assumption was made to reduce computation time but may be incorrect as it no longer calculates the velocity profile and rheology for every height. This leads to the main research question of this thesis:

•Is the assumption made to reduce calculation time in the previous version of the simulation code valid?

In this thesis the different approaches to the simulations will be investigated. Specifically the part where the assumption is made in the simulation will be adjusted. When the code is rewritten it will be benchmarked with the Newtonian fluid, water. From this fluid the rheology is known and thus is suitable as a benchmark case. Then the assumption made in the original simulation can be checked. If the assumption was incorrect the original code should no longer be used. If the assumption however is correct this code can still be used as it reduces computation time.

This thesis is divided in chapters for clarity. In the next chapter a theoretical foundation will be laid. In this chapter the most important concepts will be explained. Then, in chapter three, the numerical method will be discussed. In this chapter the important steps taken to write the code for the simulation will be explained. The way the code is checked will also be explained in this chapter. The fourth chapter will contain the results and the discussion. Here all the found results will be shown, explained and discussed. In the final chapter a conclusion will be given. There will also be an recommendation for further research.

2. Theory

In this chapter the theoretical background needed for this thesis will be explored. Firstly the background of the waveguide set-up is discussed. Following that the rheology of two different groups of fluids will be described and how the energy loss is coupled to the waveguide set-up. Then the Navier-Stokes equations will be simplified for this application.

2.1. Waveguide

As mentioned in Chapter 1 an ultrasonic waveguide viscometer will be used. This waveguide will be a thin stainless steel rectangular plate with a transducer on top as shown in Figure 1.2. This waveguide has a width W $[m]$ in the x direction, a length l in the z direction and a thickness h $[m]$ in the y direction. The transducer will generate shear waves in the waveguide that travel in the z direction and are polarized in the x direction. These waves have a propagation velocity of c_s $[m/s]$ in the z direction and have the form $U(z,t)$ $[m]$ at position z and time t. Where $U(z,t)$ can be described by the following equation:

$$U(z,t) = A(z) \cdot sin(kz - \omega t) \tag{2.1}$$

where $A(z)$ $[m]$ is the amplitude dependent on the height, $k = 2\pi/\lambda$ $[1/m]$ is the wavenumber and ω $[1/s]$ is the angular frequency. At the surface of the plate the shear waves exert a shear-stress on the fluid, causing a velocity profile in the fluid. Because of this stress, the wave in the plate loses energy. This process is called viscous dissipation and causes an amplitude attenuation. The local velocity in the x direction at the surface can be described using the following equation:

$$v_x \mid_{y=0} = B(z) \cdot cos(kz - \omega t) \tag{2.2}$$

where $B(z)$ $[m/s]$ is the velocity amplitude. From now on $B(z)$ will be referred to as *the amplitude*

Cegla [6] wrote in his research that for a range of frequency product only one shear mode can exist. The frequency thickness product range is 0-1.5 MHz mm as seen in Figure 2.1 Also in this range the phase velocity of the wave is constant. Therefore it is a non dispersive wave. Shear-waves have the advantage that the attenuation of the amplitude can directly attributed to viscosity [8].

2.2. Rheology

As stated above, the viscosity of the fluid can be linked to the energy loss of the shear-wave. However the viscosity does not have to be constant everywhere. One important factor is the shear-rate, the velocity gradient due to the shear-wave. There are fluids of which the viscosity is independent on the shear-rate, Newtonian fluids, and fluids of which the viscosity is dependent

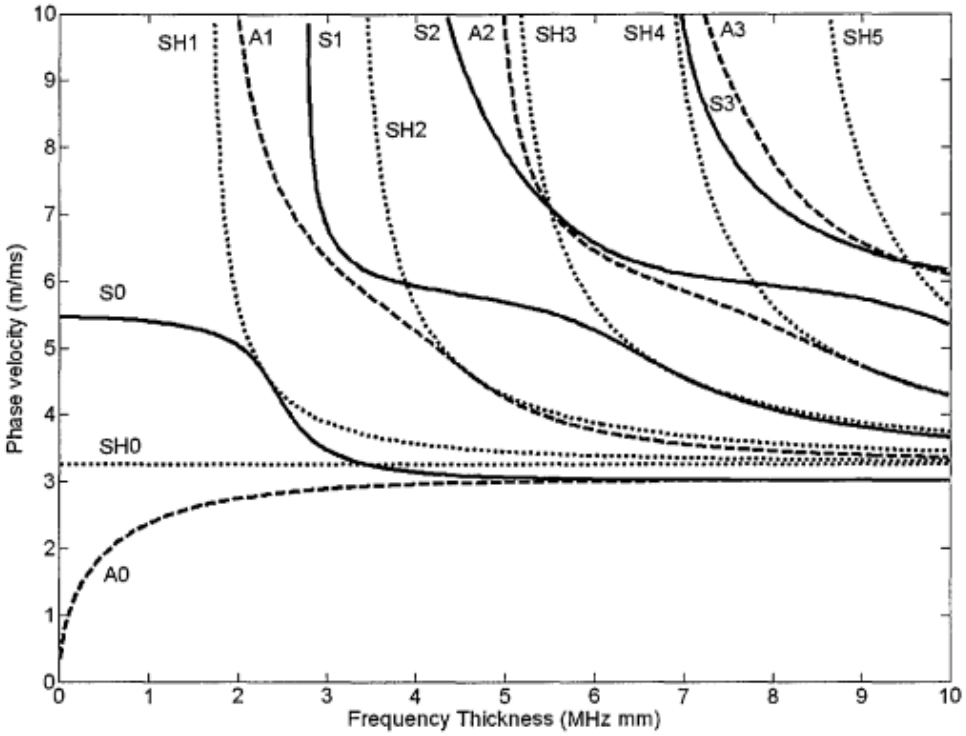

Figure 2.1.: The phase velocity for different modes against the frequency thickness in a waveguide. With SH meaning the shear-wave modes, A meaning the flexural wave modes and S meaning the compressional wave modes. [6]

on shear-rate, non-Newtonian fluids. This last group consist of a lot of different type of fluids. In this thesis the non-Newtonian Power-law fluids will be explored. An important relation is the relation of shear-stress and shear-rate. For a Newtonian fluid, in one dimension, it is [13]:

$$\tau_{yx,N} = -\mu \frac{dv_x}{dy} \tag{2.3}$$

where τ_{yx} $[Pa]$ is the shear-stress. The subscript describes that the stress is in the x direction and the stress is effecting the fluid in the y direction. μ $[Pa \cdot s]$ is the dynamic viscosity and v_x $[m/s]$ is the velocity in the x direction. For the case of a Power-law fluid the formula, in one dimension, becomes [13]:

$$\tau_{yx,P} = -K_m \left| \frac{dv_x}{dy} \right|^{m-1} \frac{dv_x}{dy} \tag{2.4}$$

where K_m $[Pa \cdot s^n]$ is the consistency and m $[-]$ the flow index.

Often an apparent viscosity is used when working with Power-law fluids [13]:

$$\mu_{app} = K_m \left| \frac{dv_x}{dy} \right|^{m-1} = K_m \dot{\gamma}^{m-1} \tag{2.5}$$

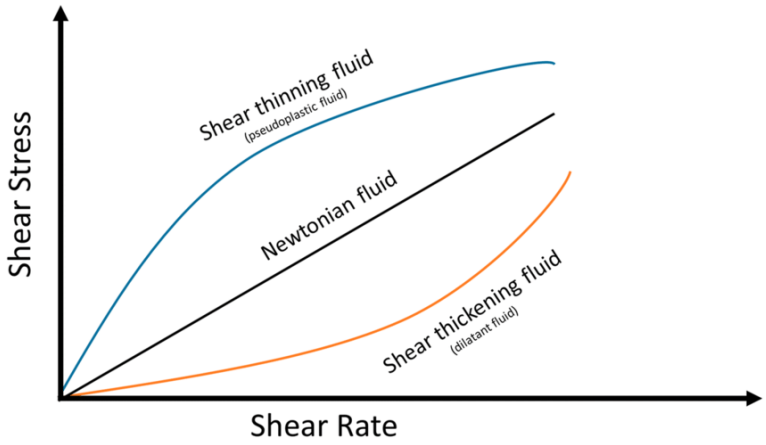

Figure 2.2.: The shear-stress against shear-rate for shear thinning, shear thickening and Newtonian fluids [14].

where $\dot{\gamma}$ $[s^{-1}]$ is the shear-rate. Shear-rate, in one dimension, can be defined as the following:

$$\dot{\gamma} = \frac{dv_x}{dy} \tag{2.6}$$

Making the formula for a Power-law fluid, in one dimension:

$$\tau_{yx,P} = -\mu_{app}\dot{\gamma} \tag{2.7}$$

Note that when $m = 1$ is used in equation 2.4 the equation for a Newtonian fluid is retrieved. When $m < 1$ this fluid is shear-thinning. This means that when the shear-rate increases the apparent viscosity decreases. With $m > 1$ this fluid is shear-thickening and when the shear-rate increases the apparent viscosity also increases [13]. In Figure 2.2 shear-stress is plotted against shear-rate for different types of fluids.

2.3. Power loss due to viscous dissipation

There needs to be an expression to link the attenuation of the shear-wave to the rheology. For a waveguide with width W $[m]$ in the x direction and an infinitesimal small length dz $[m]$ the power loss at the surface is ΔP $[W]$ [7]:

$$\Delta P_\tau = -2 \cdot \tau_0(z,t) \cdot v_x \cdot W \cdot dz \tag{2.8}$$

where $\tau_0(z,t)$ $[Pa]$ is the shear-stress at the surface and v_x $[ms^{-1}]$ is the velocity of the shear-wave polarized in the x direction at the surface. There is a factor two because energy is lost at both sides of the waveguide. Energy loss at the bottom of the waveguide can be neglected because this area is much smaller. Also energy loss due to air can be neglected. Lastly internal friction will be neglected due to the elasticity of the waveguide [7].

The full derivation can be found in Appendix A. The result is the following [7]:

$$B(z)\frac{dB(z)}{dz} = \frac{1}{\rho_s c_s h} \cdot \frac{1}{T}\int_T -2 \cdot \tau_0(z,t) v_x(y=0,z,t)dt \tag{2.9}$$

where ρ_s is the density of the waveguide $[kgm^{-3}]$, c_s is the propagation velocity in the waveguide $[ms^{-1}]$, h is the thickness of the waveguide $[m]$ and T is the period of the wave $[s]$

2.3.1. Solution for Newtonian fluid

For a Newtonian fluid an analytical solution for the velocity profile and thus τ_0 exists from stokes second problem. This solution is [15]:

$$v_x(y,z,t) = B(z)e^{-y/\delta} \cdot cos(\omega t - y/\delta) \tag{2.10}$$

where $\delta = (\frac{2\mu}{\omega\rho_f})^{1/2}$ $[m]$ is the viscous skin depth.

At first sight, Stokes second problem does not apply in this situation because not the whole wall is oscillating. However this solution can still be used because $\delta << \lambda$ and thus the velocity gradient in the z direction has insignificant influence as $\frac{dv_x}{dy} \approx \frac{v_x}{\delta} >> \frac{dv_x}{dz} \approx \frac{v_x}{\lambda}$ [7]. When this is substituted in equation 2.9 the following relation can be found:

$$B(z) = B_0 \cdot exp(-\frac{\mu}{\delta\rho_s c_s h} \cdot z) = B_0 \cdot exp(\alpha \cdot z) \tag{2.11}$$

where B_0 $[m]$ is the initial amplitude at $z = 0$. The relation between the amplitude and the height should be a decaying exponential.

However for Power-law fluids there is no analytical solution for the velocity profile from stokes second problem. An alternative expression for the velocity profile or the shear-rate should be explored to solve equation 2.9.

2.4. Navier-Stokes equations

The Navier-Stokes equations describe the time-dependent three dimensional flow of in-compressible fluids [13].

$$\rho\frac{\partial \boldsymbol{v}}{\partial t} = -\rho\boldsymbol{v} \cdot \boldsymbol{\nabla v} - \boldsymbol{\nabla} \cdot\boldsymbol{\tau} - \boldsymbol{\nabla} p + \rho\boldsymbol{g} \tag{2.12}$$

where ρ is the density of the fluid $[kgm^{-3}]$, $\boldsymbol{v}$ is the velocity vector in the fluid $[ms^{-1}]$, $\boldsymbol{\tau}$ is the shear-stress tensor $[Pa]$, p is the pressure $[Pa]$ and $\boldsymbol{g}$ is the gravity vector $[ms^{-2}]$

In the specific case of the proposed waveguide a lot of terms will drop out of the equation and thus the equation can be simplified.

The pressure gradient and gravity effect will become zero because the pressure and gravity do not play a role. Furthermore the generated wave only has a velocity in the x direction and thus $v_y = v_z = 0$. There is no convection in this specific case. Lastly the only non-zero shear-stress is $\tau_{yx}(y)$. The following simplification in the case of the used waveguide can be made[10]:

$$\frac{\partial v_x}{\partial t} = -\frac{1}{\rho_f}\frac{\partial \tau_{yx}}{\partial y} \tag{2.13}$$

This equation can be used in the numerical simulation of the waveguide to retrieve the velocity gradient.

3. Numerical method

In this chapter the numerical method will be discussed. First it will be discussed how the simulation code will be made. Secondly the manner of testing the simulation and retrieving the results will be discussed.

3.1. Simulation code

To help the process of finding a relation between the rheology of a Power-law fluid and the amplitude attenuation a simulation code is needed. Borstlap [10] developed a simulation code that provides the $B(z)$ for different fluids. However this code needs to be reviewed to check the validity of an assumption that was made. When the code is checked and rewritten the new code can be tested. This code will be written in the programming language Python. This language is open source and has many useful math and physics libraries that can be used.

3.2. The usage Ix and X

Borstlap [10] introduces variables I_x and X to improve computing time in her simulation.

$$X(z) = \frac{1}{B^{m+1}} \tau_{yx,0}(z,t) v_{x,0}(z,t) \tag{3.1}$$

$$I_x = \frac{2}{T} \int_T X(z,t) dt \tag{3.2}$$

She states that because $X(z,t)$ is expected to be periodic, I_x needs to be calculated for only one value of z because it will give the same result for every z. By using these dummy variables she stated that it was no longer needed to calculate τ_0 and $v_{x,0}$ for every z to calculate $B(z)$ with equation 2.9. However the assumption on which this is based is that $\tau_{yx,0}$ scales with $B(z)^m$. This assumption is not straight forward and needs further investigation. Now for every discrete step in the z direction $\tau_{yx,0}$ and $v_{x,0}$ needs to be calculated and thus the computing time will be increased significantly. To reduce this computing time less steps can be taken in the z direction.

3.3. Approach

In this section the new approach will be explained. As discussed above for every height $v_{x,0}$ and $\tau_{yx,0}$ need to be calculated. The waveguide will be discretized in the z and y direction. This will be explained further in the next section. The discretization is schematically shown in Figure 3.1.

First the shear-rate and shear-stress will be calculated for the first height slice and for every y. When this is done the velocity profile can be calculated for that height slice. From this profile

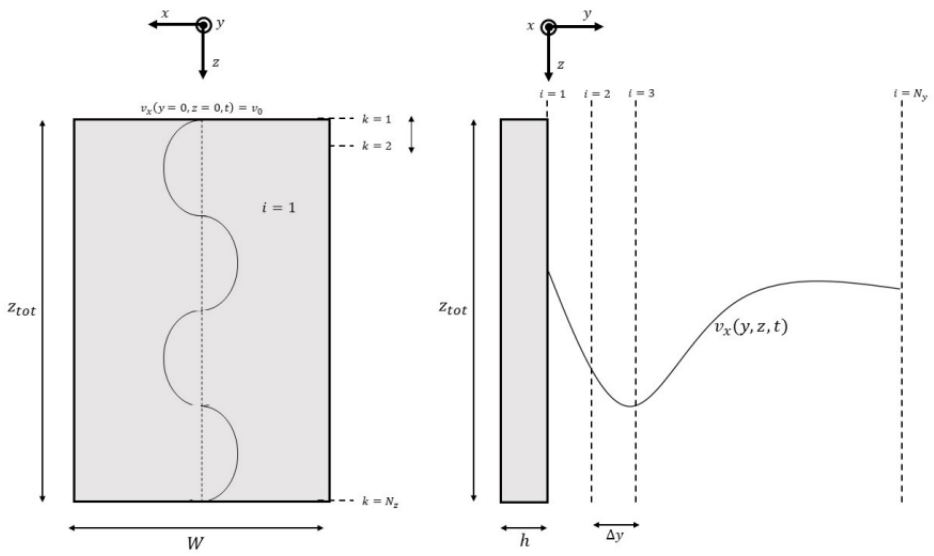

Figure 3.1.: A schematic view of the numerical waveguide set-up [10].

and the shear-stress, with equation 2.9, the amplitude of the next height slice will be calculated. Then the velocity at the surface of the waveguide is known and the shear-rate and shear-stress of the next slice can be caculated. This is repeated until the whole plate is simulated. To calculate the shear-rate, shear-stress, velocity and the amplitude equations 2.5, 2.9 and 2.12 will be used.

The biggest difference with the simulation used by Borstlap and Schuringa is that for every z, the velocity profile, shear-rate and shear-stress is calculated again and the velocity is dependent on the calculated amplitude. Borstlap and Schuringa both used equations 2.5 and 2.12 for the simulation. However since $X(z)$ and I_x are no longer used, equation 2.9 had to be discretized in another way. One big disadvantage of the new approach is that this takes a significantly longer computation time and the simulation needs a lot of memory to store all the results. To decrease the amount of storage needed the velocity profile, shear-rate and shear-stress will only be saved for the last iteration, so the last z at the last ω.

3.4. Discretization and discrete notation

Discretization of a function is when a continuous space is divided in points $[x_i, f_i]$ with a discrete distance, h. This way integrals en differential equations can be approximated in numerical simulations. Commonly used methods to approximate derivatives are the finite difference methods. One of the finite difference method is the central linear finite difference method [16]:

$$f^{'}(x_i) \approx \frac{f_{i+1} - f_{i-1}}{2h} \tag{3.3}$$

This is the most commonly used approximation. The disadvantage of this formula is the term f_{i-1}. It is not possible to calculate the derivative of the first point. In that case, the second order forward finite difference method can be used [16]:

$$f^{'}(x_i) \approx \frac{-3f_i + 4f_{i+1} - f_{i+2}}{2h} \tag{3.4}$$

Partial derivatives in time can be approximated by the following[10]:

$$f^{'}(t_n) \approx \frac{f_{n+1} + f_n}{\Delta t} \tag{3.5}$$

Because both spatial and time derivatives will be used it is important to have a clear notation. In this thesis the following discrete notation will be used:

$$a^n_{i,k} = a(y_i, z_k, t_n) \tag{3.6}$$

with $t_n = n\Delta t$, $y_i = i\Delta y$ and $z_k = k\Delta z$

Set of discretized equations

Using this notation and the approximations described above, formulas 2.5, 2.9 and 2.12 can discretized. This results in the following equations. First equation 2.12 can be approximated by:

$$v^{n+1}_{i,k} = v^n_{i,k} - \frac{1}{\rho_f}\frac{\Delta t}{2\Delta y}(\tau^n_{i+1,k} - \tau^n_{i-1,k}) \tag{3.7}$$

Equation 2.5 becomes:

$$\tau^n_{i,k} = \frac{-K_m}{(2\Delta y)^m}\left|(-3v^n_{i,k} + 4v^n_{i+1,k} - v^n_{i+2,k})\right|^{m-1}(-3v^n_{i,k} + 4v^n_{i+1,k} - v^n_{i+2,k}) \tag{3.8}$$

Where $\dot{\gamma}$ is described by:

$$\dot{\gamma}^n_{i,k} = (-3v^n_{i,k} + 4v^n_{i+1,k} - v^n_{i+2,k})/(2\Delta y) \tag{3.9}$$

Simplifying for $\dot{\gamma}^n_{i,k} > 0$

$$\tau^n_{i,k} = -K_m\left(\frac{(-3v^n_{i,k} + 4v^n_{i+1,k} - v^n_{i+2,k})}{(2\Delta y)}\right)^m \tag{3.10}$$

When $\dot{\gamma}^n_{i,k} < 0$ the simplification becomes:

$$\tau^n_{i,k} = K_m\left(\frac{-(-3v^n_{i,k} + 4v^n_{i+1,k} - v^n_{i+2,k})}{(2\Delta y)}\right)^m \tag{3.11}$$

Lastly equation 2.9 can be approximated by:

$$B_{i,k+1} = B_{i,k} - \frac{\Delta z}{\rho_s c_s h T B_{i,k}}\int_T 2\tau^n_{0,k}v^n_{0,k}dt \tag{3.12}$$

The integral will be calculated using the the trapezoidal method. This will be implemented by using a Python NumPy function np.trapz($2\tau^n_{1,k}v^n_{1,k}, t$) [17].

3.5. Flow chart

A flow chart is a schematic view of the structure of the simulation. This is useful to gain understanding of the code. In figure 3.2 the flow chart of this code is shown.

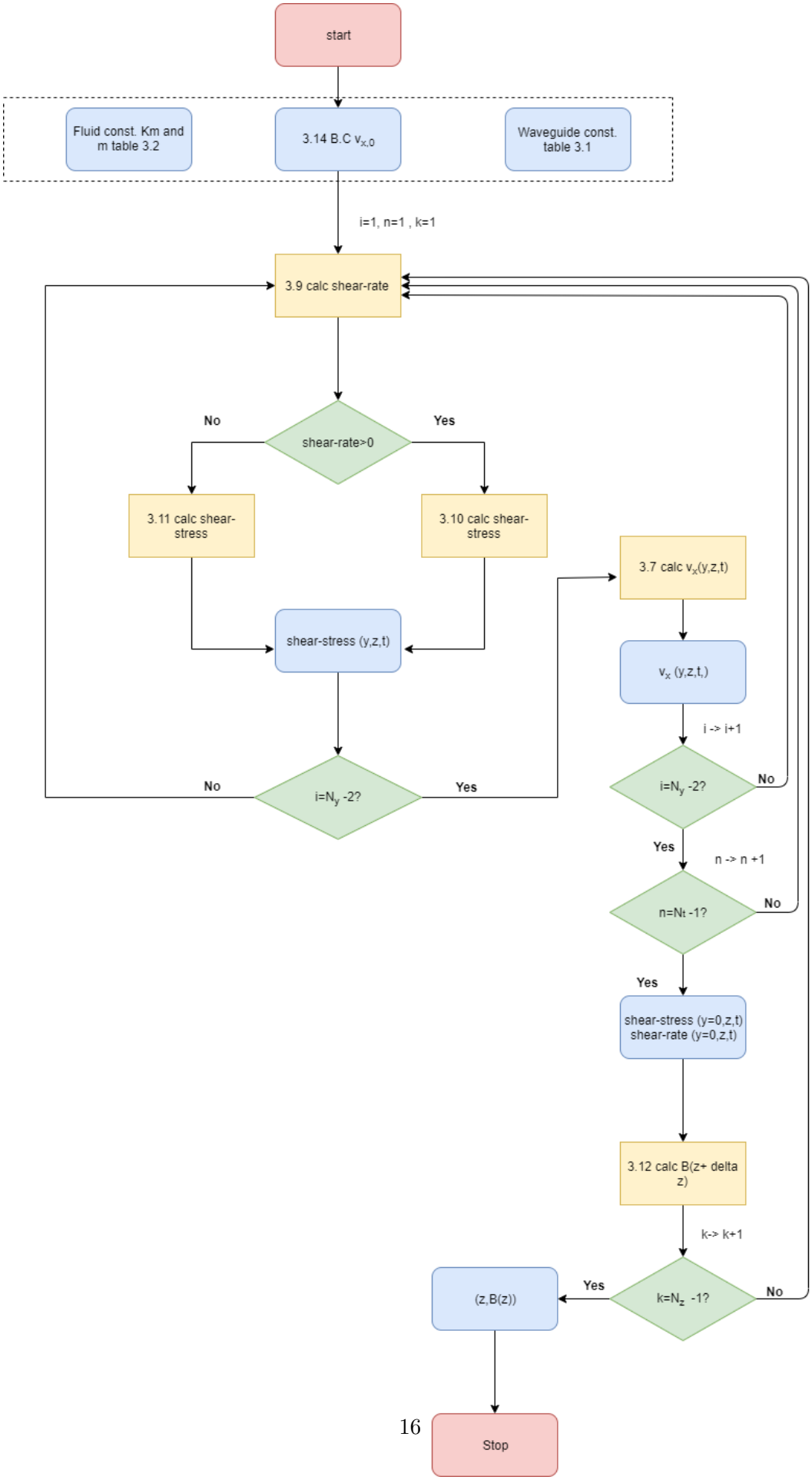

Figure 3.2.: The flow chart of the changed code simulating the wave guide setup with $B(z)$ as product.

3.6. Constants

In the code different constants will be used. In this section an overview of these constants will be given. First the constants determined by the waveguide. Rook [8] performed the waveguide measurements on Newtonian fluids and measured different constants. These are shown in table 3.1. The chosen frequency thickness product is smaller then 1.5 MHz mm as described in section 2.1. This frequency range is also the range where the energy loss in the waveguide as a result of frequency is the lowest as stated by Rook [8]. The used fluid determines other constants. An overview for different fluids is given in table 3.2.

Table 3.1.: Constants used for the simulation determined by the waveguide experiment [8].

$h[m]$	$l[m]$	$W[m]$	$\rho_s[kgm^{-3}]$	$c_s[ms^{-1}]$	$f[Hz]$
$202 \cdot 10^{-6}$	$203.5 \cdot 10^{-3}$	0.0802	7876	3083	$3.3 \cdot 10^6 - 3.7 \cdot 10^6$

Table 3.2.: Fluid constants used for the simulation. The values for soybean oil where retrieved from [18], for ketchup from [19], for ethylene glycol from [20] and for water from [21].

Fluid	$m[-]$	$K_m[Pas^m]$	$\rho_f[kgm^{-3}]$
Water	1	0.001	997
Ketchup	0.3	6.47	1136
Soybean oil	0.51	2.18	930
Ethylene glycol	1.29	0.0011	1110

Schuringa [11] notes the importance of the used time period. Because the flow is still developing in the fluid during the first period it is more accurate to simulate 16 periods as the flow is stabilized. However this increases computation time. A time period of 8 periods is chosen as balance between accuracy and computation time.

3.7. Boundary conditions

Furthermore it is important to set boundary conditions. At $t = 0$ the fluid is at rest. The boundary conditions in discrete form are given:

for $y_i > 0$:

$$v_{i,k}^{n=1} = 0 \tag{3.13}$$

for $t_n > 0$:

$$v_{i=1,k}^{n} = B_{i=1,k}^{n} cos(\omega t_n) \tag{3.14}$$

for $y_i \to \infty$

$$v_{i,k}^{n} \to 0 \tag{3.15}$$

Lastly

$$B_{k=1}^{n} = v_0 \tag{3.16}$$

Where in this thesis $v_0 = 0.08$ $[m/s]$ is chosen. This was chosen as the largest frequency used was $f = 3.7$ MHz, then amplitude of the shear-wave $A(z)$ would be in the order of 3 nm.

3.8. Stability and convergence

Because numerical approximations of derivatives are used it is important to take a look at the stability of the simulation. For Newtonian fluid a stability condition exists [10]:

$$\frac{1}{\rho_f}\frac{\Delta t}{\Delta y^2} \leq \frac{1}{2} \tag{3.17}$$

Which can be found by substituting equation 3.8 in equation 3.7 for $m = 1$. Note that for Power-law fluids the stability is not determined by [10]:

$$\frac{1}{\rho_f}\frac{\Delta t}{\Delta y^{m+1}} \leq \frac{1}{2} \tag{3.18}$$

But this can be used as a starting point. By trial and error Borstlap [10] found the values for Δy and Δt for which the simulation is stable. Δy depends strongly on the fluid and its rheological properties and will be determined for every fluid and frequency independently. Δt will be determined depending on the frequency used.

Next to stability one wants the results to converge to a value, if known the literature value. This can be achieved by choosing the step sizes as small as possible. The disadvantage is that this increases the computation time and storage. How the step sizes are calculated is explained in Appendix B. In this thesis there will be iterated over z as well. For the step size the following is chosen: $\Delta z = \lambda = c_s/f$. There will be as many steps in de z direction as it takes to compute the whole waveguide.

3.9. Benchmark

To check if the simulation is accurate a benchmark is performed. The fist check will be trying to retrieve the known relation for the amplitude and the immersion depth for a Newtonian fluid. For Newtonian fluids an exponential decay of the amplitude is expected. This will be checked by using the fluid properties for water as given in Table 3.2 in the simulation and plotting the amplitude against the immersion depth.

The second benchmark will be checking if the step size in the z direction is acceptable. In this benchmark the velocity profile will be plotted for different step sizes, $\Delta z = \lambda$, $\Delta z = \lambda/2$, $\Delta z = \lambda/4$ and $\Delta z = \lambda/8$, to check if the results converge. These simulations will be performed with less steps in the z direction to reduce computation time.

3.10. Validation of the assumption

The assumption made by Borstlap [10] discussed in section 3.2 should be checked. She states that $\tau_{yx,0}$ scales with $B(z)^m$. To check this a plot will be made where $\tau_{yx,0}(z,t)$ is plotted against $B(z)^m$. This is done for different values of t: $t = 1/2\pi/\omega$, $t = \pi/\omega$ and $t = 3/2\pi/\omega$. If the assumption is correct a linear relationship will be shown. This will be repeated for three different fluids: soybean oil, ketchup and ethylene glycol.

3.11. Retrieving m and K_m

Rohde [7] proposed a way to retrieve m and K_m that Borstlap [10] and Schuringa [11] both investigated. The values for m and K_m are retrieved by fitting the numerical data $[z, B(z)]$ to the following linear function for a fixed frequency of $f = 3.7$ MHz:

$$\Delta B^* = K_m \Delta z^* \tag{3.19}$$

in which:

$$\Delta B^* = \left| B(z)^{1-m} - B_0^{1-m} \right|^{2/(2-m)} \tag{3.20}$$

$$\Delta z^* = \left(\frac{2P_3(m)}{\rho_s c_s h} |1-m| \cdot (\omega \rho_f)^{1/2} \cdot z\right)^{2/(2-m)} \tag{3.21}$$

Then m needs to be varied to find K_m. Data sets B^* and z^* are calculated for a range of m values. Then the data is linearly fitted to $y = a \cdot \Delta z^* + b$ using the np.polyfit function from the NumPy libary [22]. The value of m for which the fitting error is the smallest is the found value of m. The fit error is described by:

$$\epsilon(m_{fit}) = \sum^{Nz} \sqrt{(y_{fit}(z, m_{fit}) - \Delta B^*(z, m_{fit}))^2} \tag{3.22}$$

where Nz the amount of steps in the z direction.

When the value of m is found, and thus the error is minimized, the value of K_m can be found as $a = K_m$. For soybean oil and ketchup m will range from 0.1 to 0.995 in 200 steps. For ethylene glycol m will range from 1.005 to 1.9 in 200 steps.

4. Results and discussion

In this chapter the results will be shown, explained and discussed. First the benchmark cases will be discussed. Then the found rheology for different fluids will be discussed. For clarity, the code used by Borstlap and Schuringa will be referred as the *previous* version of the code. The version of the code written in this thesis will be referred as the *current* version of the code.

4.1. Water benchmark

First the code needed to be benchmarked. This was done by using the simulation with water and looking at the relation between $B(z)$ and z. An exponential decay was expected as stated in section 2.3.1. The goal is to find the analytically know relation from the simulation data. The simulation for $f = 3.7$ MHz was fitted with an exponential decay. The result of the simulation and the fitted relation is shown in Figure 4.1. When α from equation 2.11 is calculated it is discovered that $\alpha = -0.655$. The fitted relation was $B = exp(-2.526) \cdot exp(-0.712z)$. The found relation fitted nicely over the simulation points as can be seen in Figure 4.1. The fitted value for α, $\alpha_{fit} = -0.712$, which is not exactly the same as the theoretical value. The deviation however, is within 9% of the theoretical value. When looked at the fitted initial amplitude, $B_{0,fit} = exp(-2.526) = 0.08$, this is exactly what was expected from equation 2.11. It should be noted that this fit was performed on a small range of z. The curve of the exponential decay is hardly visible on this scale and thus it is harder to fit the relation precisely. The small range of z increases the uncertainty in the fit. To improve this the simulation could be repeated for a bigger range of z.

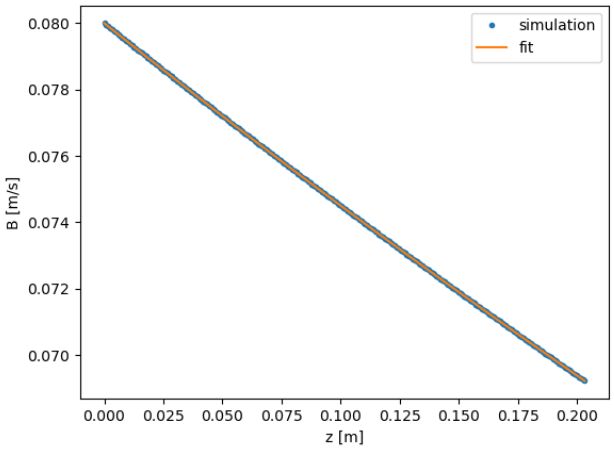

Figure 4.1.: The amplitude against the height of water for $f = 3.7$ MHz with an exponential fit of $B = exp(-2.526) \cdot exp(-0.712z)$.

4.2. Step size in the z direction

The next test was if the step size in the z direction has an significant influence on the results. To investigated this a small piece of the plate was simulated. This was done with soybean oil. First the amplitude was plotted against the height for different frequencies all starting with the same initial amplitude. The result for $\Delta z = \lambda$ is shown in Figure 4.2.

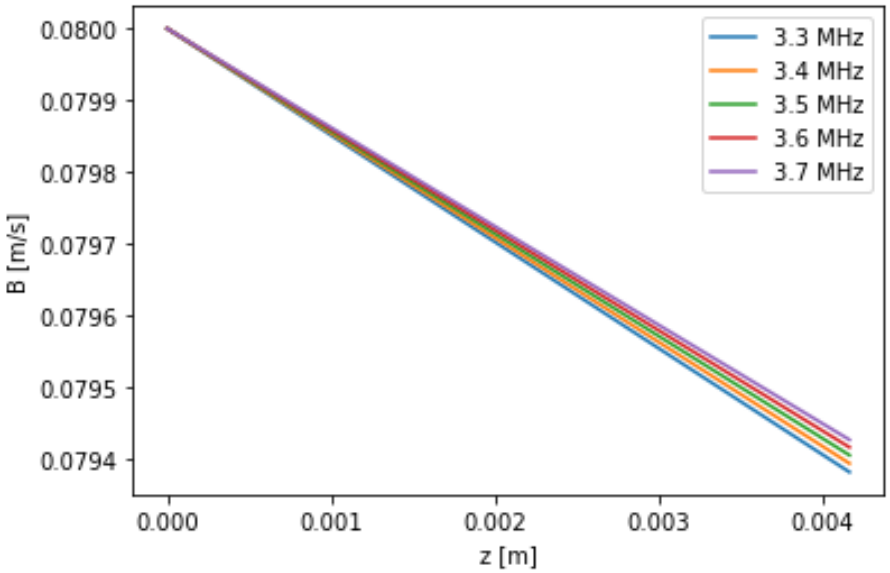

Figure 4.2.: The amplitude against the height of soybean oil for multiple frequencies with the same initial amplitude of $B(z = 0) = 0.08[m/s]$ and $\Delta z = \lambda$.

The same plot was made for $\Delta z = 0.5 \cdot \lambda$ and is shown in Figure 4.3, for $\Delta z = 0.25 \cdot \lambda$ and is shown in Figure 4.4 and lastly for $\Delta z = 0.125 \cdot \lambda$ which is shown in Figure 4.5.

Figures 4.2, 4.3, 4.4 and 4.5 look very similar. Visual inspection of the plots does not reveal differences. Therefore, as Δz is a factor in equation 3.12, a table was made in which the value of $\Delta B(z)$ is compared for $\Delta z = 2\lambda$, $\Delta z = \lambda$ and $\Delta z = \lambda/8$, and for different frequencies. $\Delta B(z)$ describes the difference in $B(z)$ at $z = 0$ m and $z = 0.004$ m. This is displayed in Table 4.1.

Table 4.1.: The amplitude difference found for different frequencies and step sizes between $z = 0$ m and $z = 0.004$ m.

Step size	f=3.3 MHz	f=3.4 MHz	f=3.5 MHz	f=3.6 MHz	f= 3.7 MHz
$\Delta z = 2\lambda$	$\Delta B = 0.00050[m/s]$	$\Delta B = 0.00049[m/s]$	$\Delta B = 0.00048[m/s]$	$\Delta B = 0.00047[m/s]$	$\Delta B = 0.00046[m/s]$
$\Delta z = \lambda$	$\Delta B = 0.00062[m/s]$	$\Delta B = 0.00061[m/s]$	$\Delta B = 0.00059[m/s]$	$\Delta B = 0.00058[m/s]$	$\Delta B = 0.00057[m/s]$
$\Delta z = \lambda/8$	$\Delta B = 0.00075[m/s]$	$\Delta B = 0.00074[m/s]$	$\Delta B = 0.00072[m/s]$	$\Delta B = 0.00071[m/s]$	$\Delta B = 0.00070[m/s]$

The difference in amplitude for the two different step sizes $\Delta z = \lambda$ and $\Delta z = \lambda/8$ is 17.3% for $f = 3.3$ MHz, 17.6% for $f = 3.4$ MHz, 18.1% for $f = 3.5$ MHz, 18.3% for $f = 3.6$ MHz and 18.6% for $f = 3.7$ MHz. It can be seen that the difference between the results of $\Delta z = \lambda/8$ and $\Delta z = 2\lambda$ are even bigger. It can be concluded change is step size has influence on the amplitude attenuation. The difference in ΔB are much smaller than the initial value.

Next the velocity profiles were plotted for the different step sizes in the z direction and for the

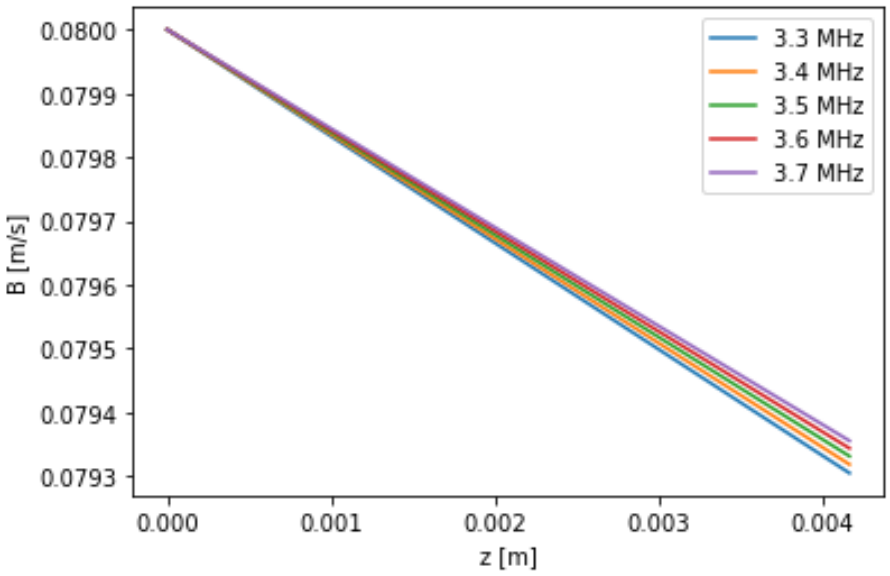

Figure 4.3.: The amplitude against the height of soybean oil for multiple frequencies with the same initial amplitude of $B(z = 0) = 0.08[m/s]$ and $\Delta z = 0.5 \cdot \lambda$.

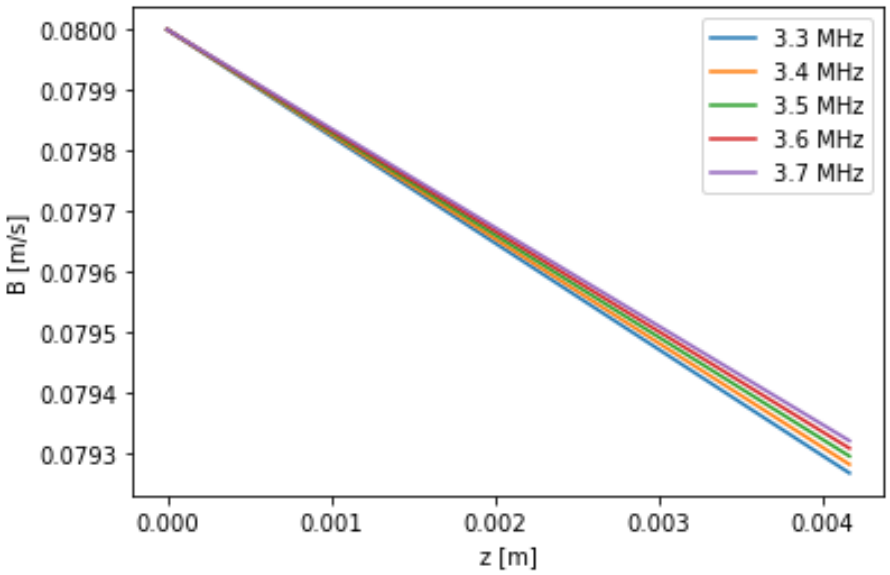

Figure 4.4.: The amplitude against the height of soybean oil for multiple frequencies with the same initial amplitude of $B(z = 0) = 0.08[m/s]$ and $\Delta z = 0.25 \cdot \lambda$.

first and second z step, $k = 1$ and $k = 2$. The velocity profiles that were plotted were at $f = 3.7$ MHz and they where plotted for different time steps.

Figures 4.6, 4.7, 4.8 and 4.9 again look very similar. In Figure 4.10 The velocity profile at $z = 0$ m was plotted for both $\Delta z = \lambda$ and $\Delta z = \lambda/8$.

No difference in velocity profile for the two different step sizes is observed in Figure 4.10. Also no numerical instability was encountered as the plots look similar in shape to the velocity

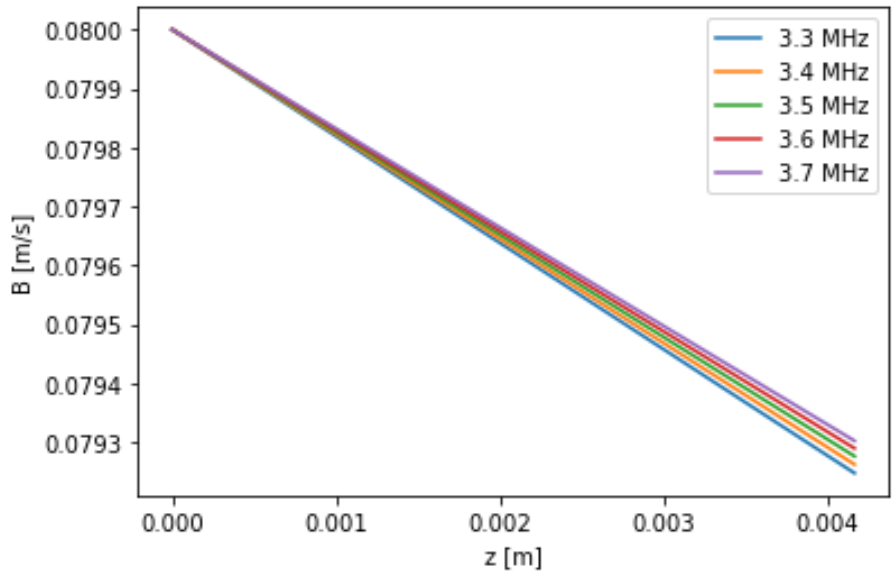

Figure 4.5.: The amplitude against the height of soybean oil for multiple frequencies with the same initial amplitude of $B(z = 0) = 0.08[m/s]$ and $\Delta z = 0.125 \cdot \lambda$.

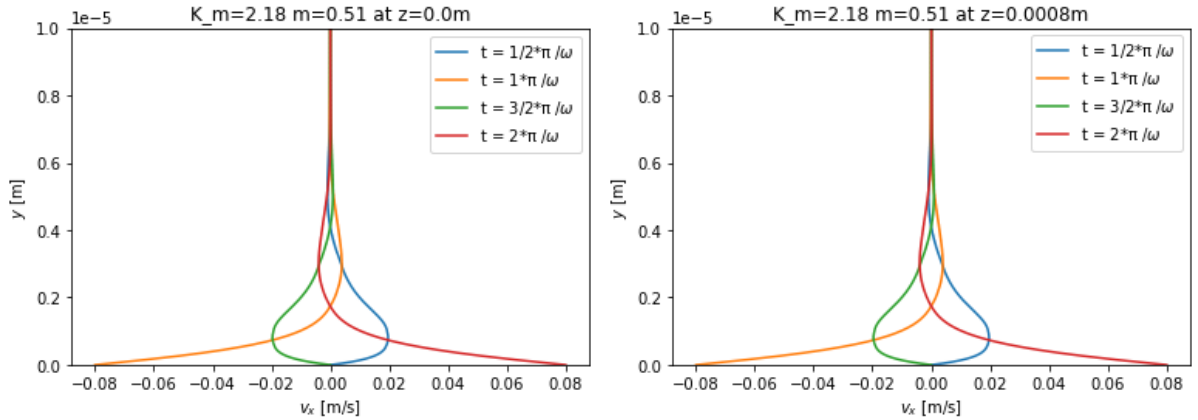

(a) The velocity profile of soybean oil at k=1.

(b) The velocity profile of soybean oil at k=2.

Figure 4.6.: The velocity profile at two different heights of soybean oil with $\Delta z = \lambda$ at $f = 3.7$ MHz.

profiles found by Borstlap [10] and Schuringa [11]. So, in conclusion, the step size has influence in the attenuation of the amplitude, but the change in the velocity profile in very small. As the computation time increases significantly by decreasing the step size, the chosen step size is $\Delta z = \lambda$ in this thesis. What could be researched in the future is what would happen is the step size would be decreased by a much bigger factor. This would have a much longer computation time but could give interesting insight in the stability. What should be noted is that the Δz used in the previous code was much bigger, about 3000 times bigger.

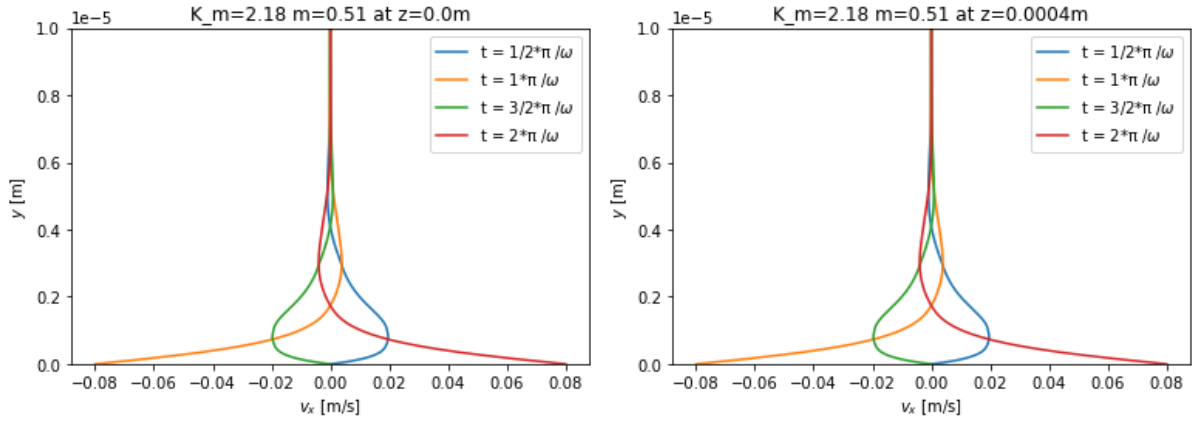

(a) The velocity profile of soybean oil at k=1.

(b) The velocity profile of soybean oil at k=2.

Figure 4.7.: The velocity profile at two different heights of soybean oil with $\Delta z = 0.5 \cdot \lambda$ at $f = 3.7$ MHz.

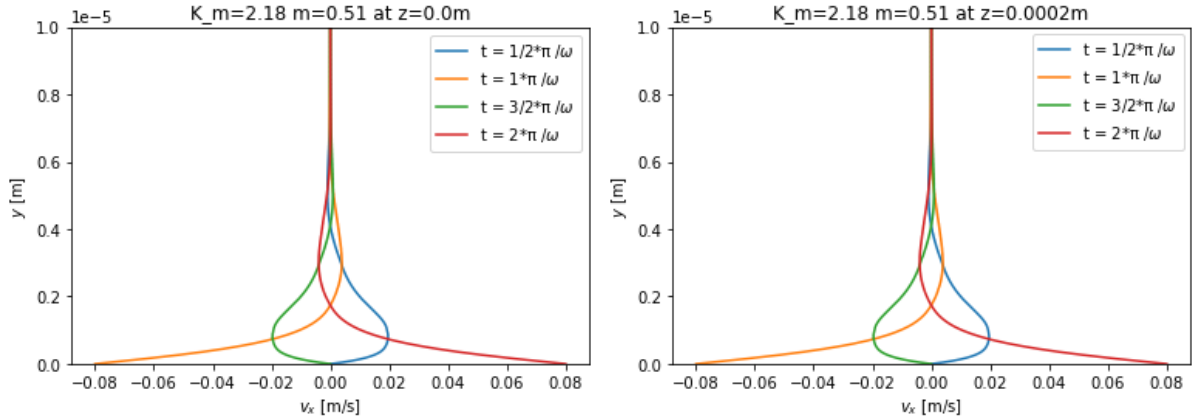

(a) The velocity profile of soybean oil at k=1.

(b) The velocity profile of soybean oil at k=2.

Figure 4.8.: The velocity profile at two different heights of soybean oil with $\Delta z = 0.25 \cdot \lambda$ at $f = 3.7$ MHz.

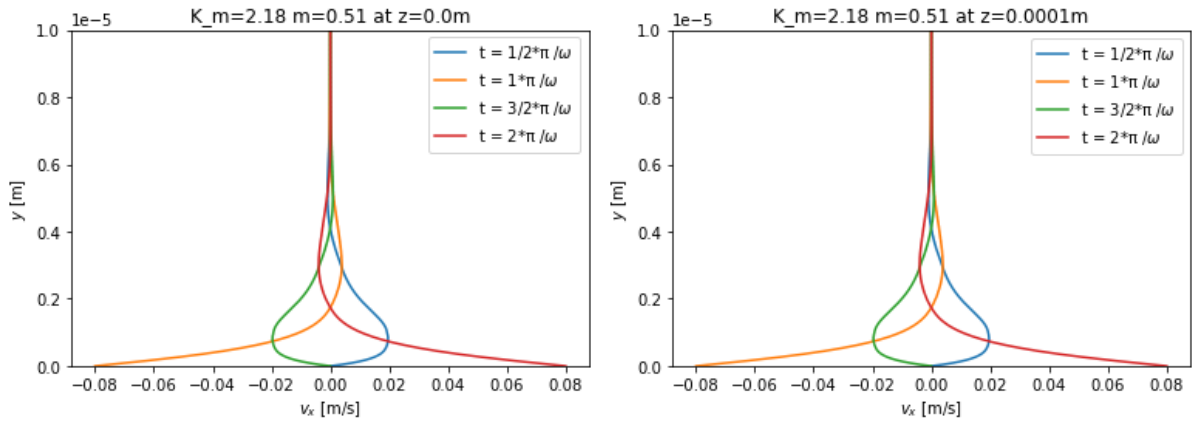

(a) The velocity profile of soybean oil at k=1.

(b) The velocity profile of soybean oil at k=2.

Figure 4.9.: The velocity profile at two different heights of soybean oil with $\Delta z = 0.125 \cdot \lambda$ at $f = 3.7$ MHz.

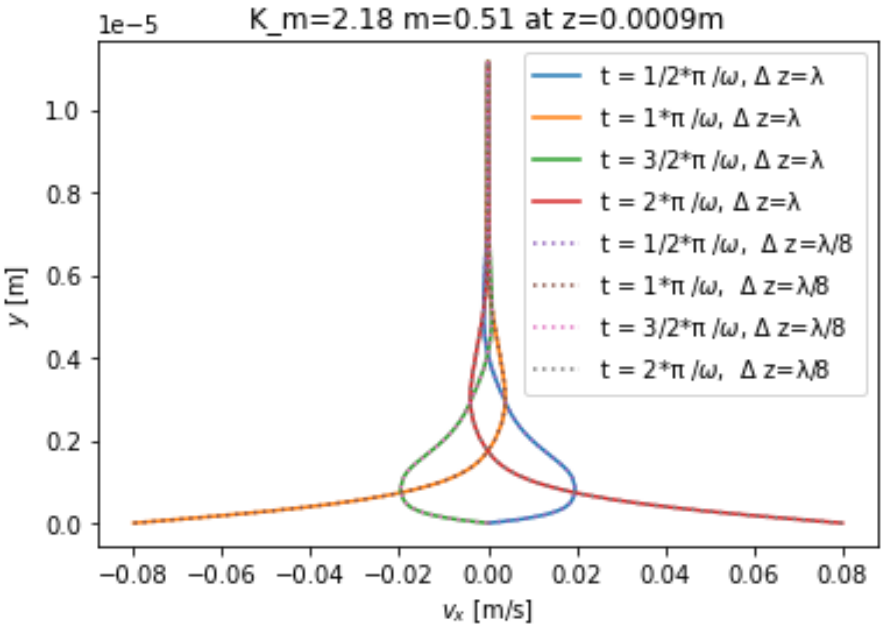

Figure 4.10.: The velocity profile at $z = 0.0009$ m for the step sizes $\Delta z = \lambda$ and $\Delta z = \lambda/8$.

4.3. Soybean oil

The first fluid that was simulated was soybean oil. First the amplitude against the height was plotted for different frequency all starting with the same initial amplitude. This is shown in Figure 4.11.

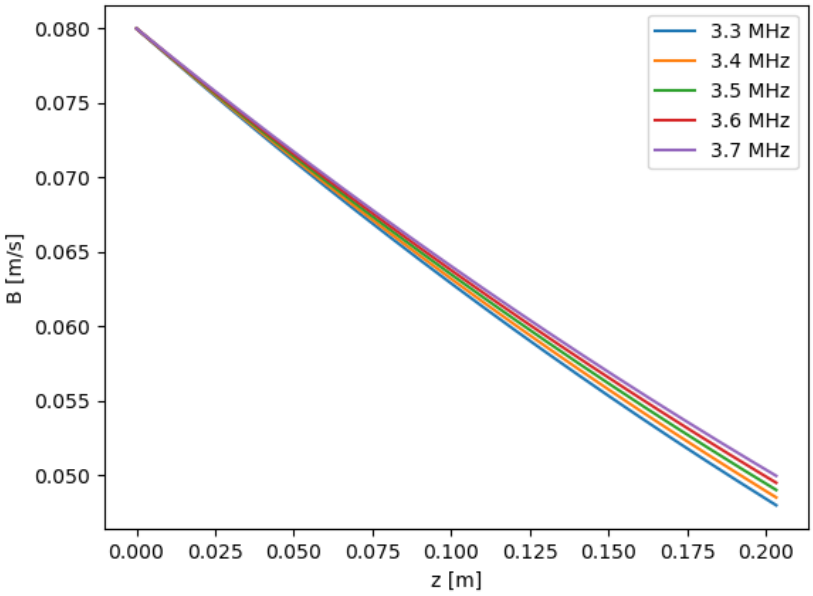

Figure 4.11.: The amplitude against the height of soybean oil for different frequencies all with initial amplitude $B(0) = 0.08[m/s]$.

In Figure 4.11 it can be seen that the amplitude attenuation is not linear as was expected. When comparing this amplitude attenuation to the amplitude attenuation of the other two fluids that are described in the next two sections, it is important to note the difference of the values on the y-axis. The different fluids have a different amount of attenuation on the same height range. This is expected as more viscous fluids have a higher attenuation as more energy is dissipated in the fluid. Therefore it was expected that ethylene glycol has the most attenuation in the used height range for all three fluids.

The shear-stress was plotted against the shear-rate to compare the shape to Figure 2.2. This is done for $f = 3.7$ MHz and displayed in Figure 4.12. The figure shows a relation that was expected for a shear-thinning fluid as shown in Figure 2.2. Lastly the shear-stress was plotted against B^m to check the assumption made in the original code. This was done for three different time steps. All three are displayed in Figure 4.13. The relation looks at first glance linear, but when examined the plots appears to be non linear. A linear fit was performed using the np.polyfit function. After that the root mean square error was calculated. For $t = 1/2 \cdot \pi/\omega$ the error was $\epsilon = 1.474$ $[m/s]$, for $t = \pi/\omega$ the error was $\epsilon = 0.7810$ $[m/s]$ and for $t = 3/2 \cdot \pi/\omega$ the error was $\epsilon = 1.358$ $[m/s]$. When $\epsilon \to 0$ the relation was indeed linear. As the errors are bigger the relation is not linear.

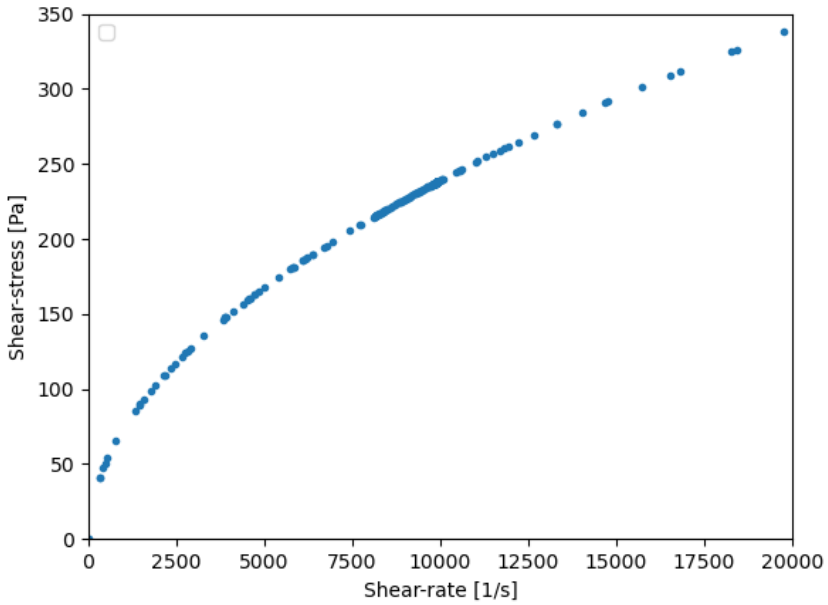

Figure 4.12.: The shear-stress against the shear-rate of soybean oil for frequency $f = 3.7$ MHz at $k = 1$.

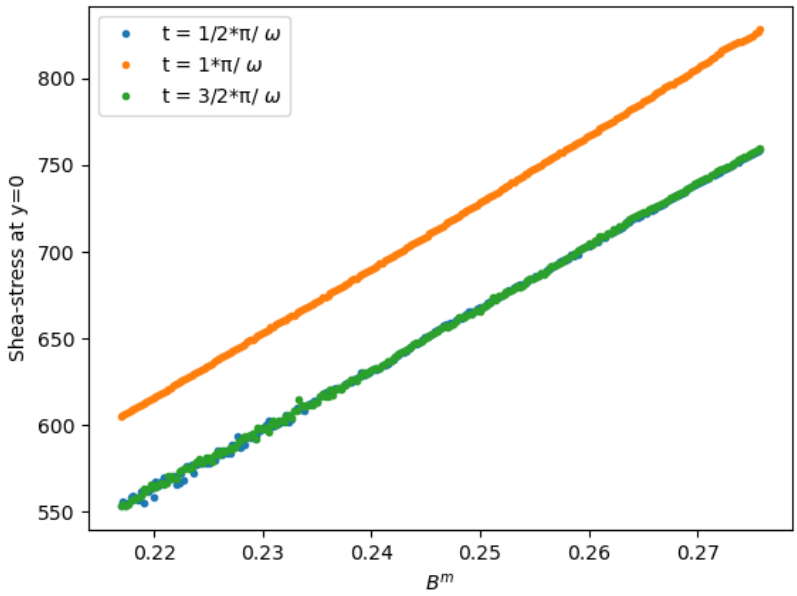

Figure 4.13.: The shear-stress against B^m of soybean oil for $f = 3.7$ MHz at $k = 1$.

4.4. Ethylene glycol

Ethylene glycol is a shear-thickening fluid. The simulation was tested for this fluid as well. First, again the amplitude against the height was plotted. This is shown in Figure 4.14.

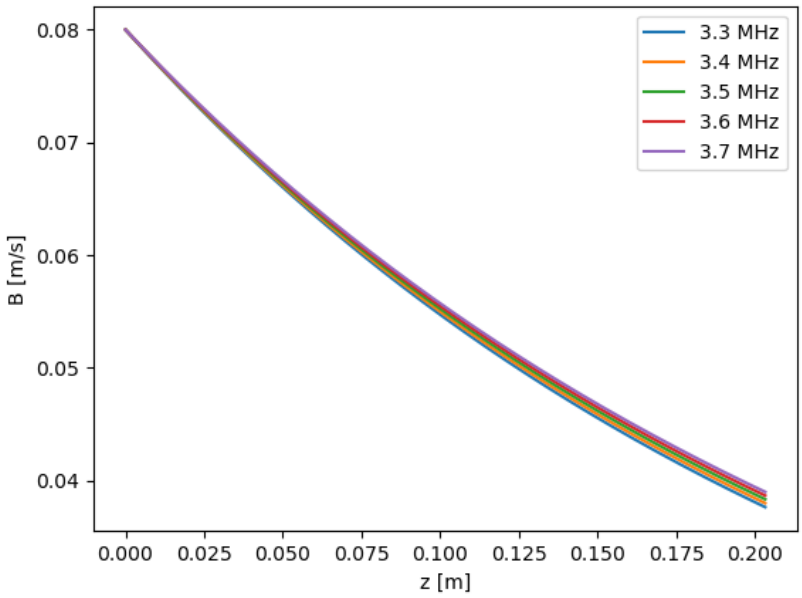

Figure 4.14.: The amplitude against the height of ethylene glycol for different frequencies all with initial amplitude $B(0) = 0.08[m/s]$.

There is an obvious non linear attenuation visible what was expected for this fluid. Indeed the amplitude attenuation is the biggest at $z = 0.2$ m for ethylene glycol as explained in the previous section.

The shear-stress was plotted against the shear-rate. The used frequency is again $f = 3.7$ MHz. This is shown in Figure 4.15. When the shape of Figure 4.15 is compared to Figure 2.2 it is clear that the shape that was found is what is expected. Lastly the shear-stress is plotted against $B(z)^m$. This is done for $f = 3.7$ MHz and shown in Figure 4.16. Again when first glanced at this figure the relation might seems linear but when inspected more closely the relation turns out to be non linear. A linear fit was performed using the np.polyfit function. After this was done the root mean square error was calculated. For the results for $t = 1/2 \cdot \pi/\omega$ and $t = 3/2\pi/\omega$ the root mean square error was $\epsilon = 3.206$ $[m/s]$. For $t = \pi/\omega$ the mean square error was $\epsilon = 3.354$ $[m/s]$.

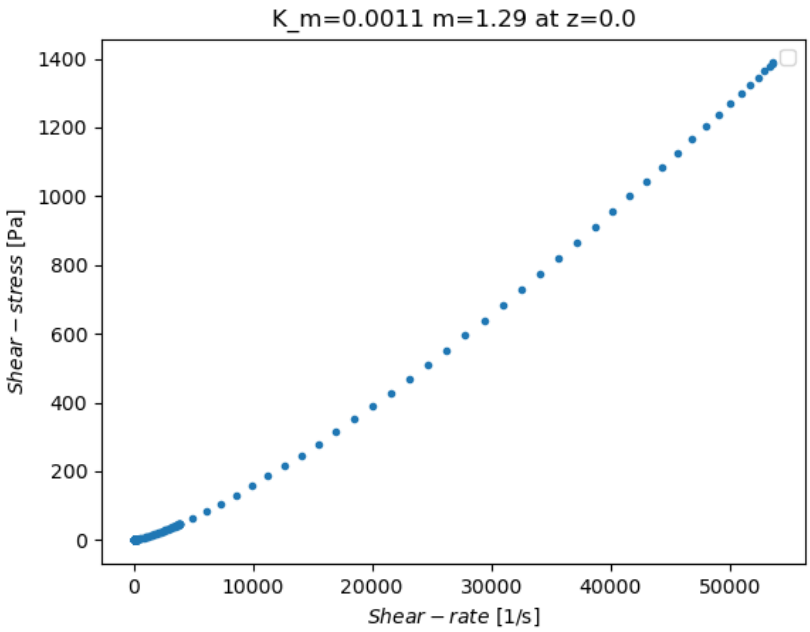

Figure 4.15.: The shear-stress against the shear-rate of ethylene glycol for frequency $f = 3.7$ MHz at $k = 1$.

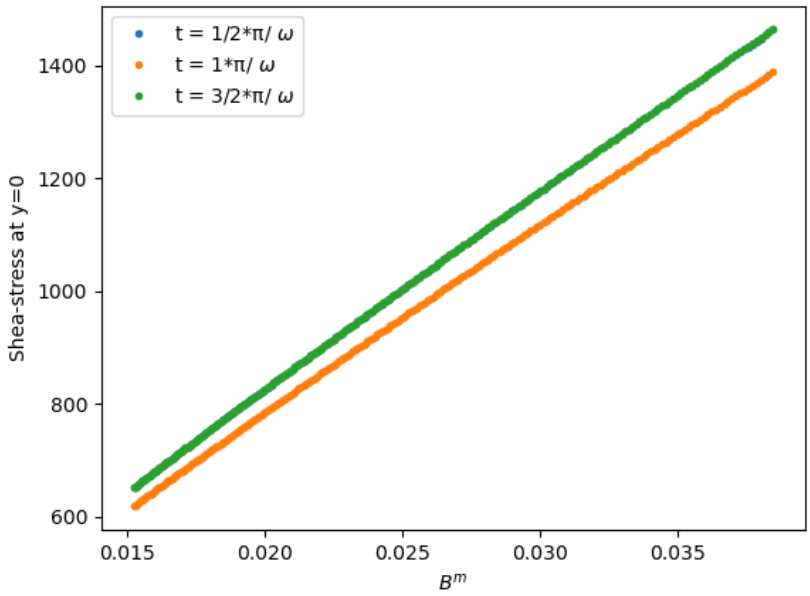

Figure 4.16.: The shear-stress against B^m of ethylene glycol for $f = 3.7$ MHz at $k = 1$.

4.5. Ketchup

Another fluid on which the code was tested was ketchup. This is like soybean oil a shear-thinning fluid. First the amplitude was plotted against the height for different frequencies. The result is shown in Figure 4.17. This appears to be a linear relation. But when examined it is

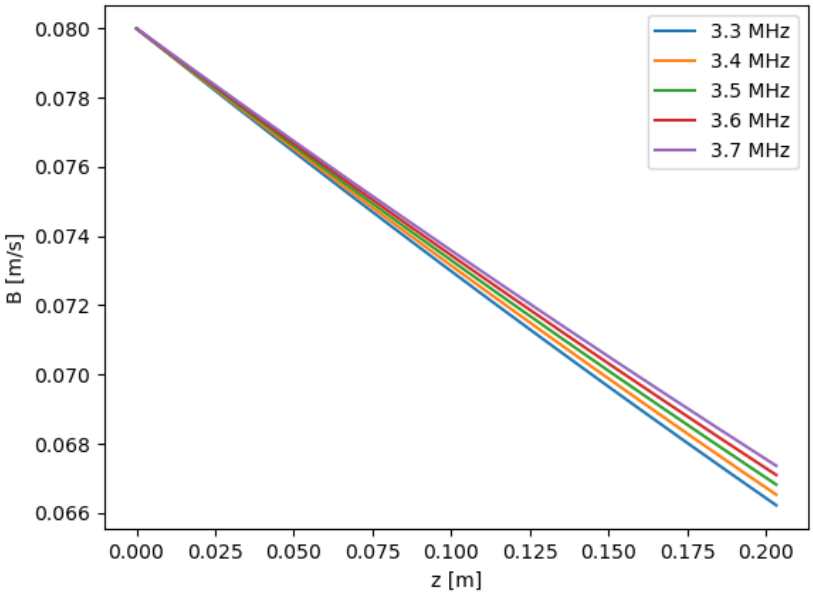

Figure 4.17.: The amplitude against the height of ketchup for different frequencies all with initial amplitude $B(0) = 0.08[m/s]$.

not quite linear. Then the shear-stress is again plotted against the shear-rate. This is done for $f = 3.7$ MHz and shown in Figure 4.18. When compared to Figure 2.2 it can be seen that the shape is again what we expect from a shear-thinning fluid. Lastly the shear-stress is plotted against $B(z)^m$ This is done for $f = 3.7$ MHz and shown in Figure 4.19.

This figure is not quite what was expected. As seen in the plots of the other fluids the measurement point lied nicely on a line whereas in this plot it is more scattered. This could possible be a numerical instability because there are differential equation approximated in the code. First the velocity profile was checked to see if there where any numerical instabilities in the y step size. This velocity profile is shown in Figure 4.20. The shape of velocity profile is as expected and no instability can be seen. To find out if the instability was caused by the step size in the z direction the simulation was performed again but now with $\Delta z = 0.25 \cdot \lambda$. The result is shown in Figure 4.21.

The points in Figure 4.21 are still very much scattered. The possible stability issue was not solved with this decrease in step size. Lastly the step size was even further decreased for a last test. Now $\Delta z = \frac{\lambda}{20}$ was used. This increased the computation time significantly to over 15 hours. The result is shown in Figure 4.22.

The simulation points in Figure 4.22 are again scattered. This graph is not physical and can not be used to make a conclusion about the validity of the approximation used in the previous

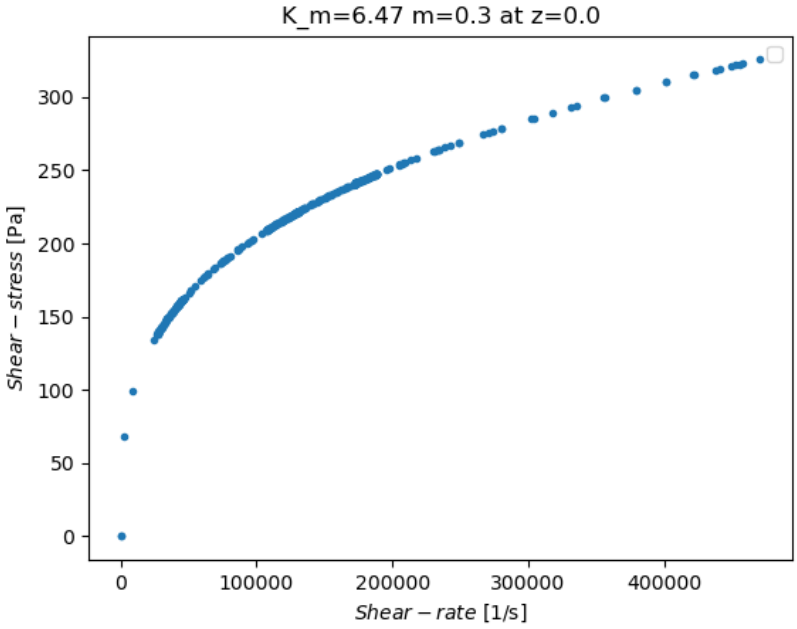

Figure 4.18.: The shear-stress against the shear-rate of ketchup for frequency $f = 3.7$ MHz at $k = 1$.

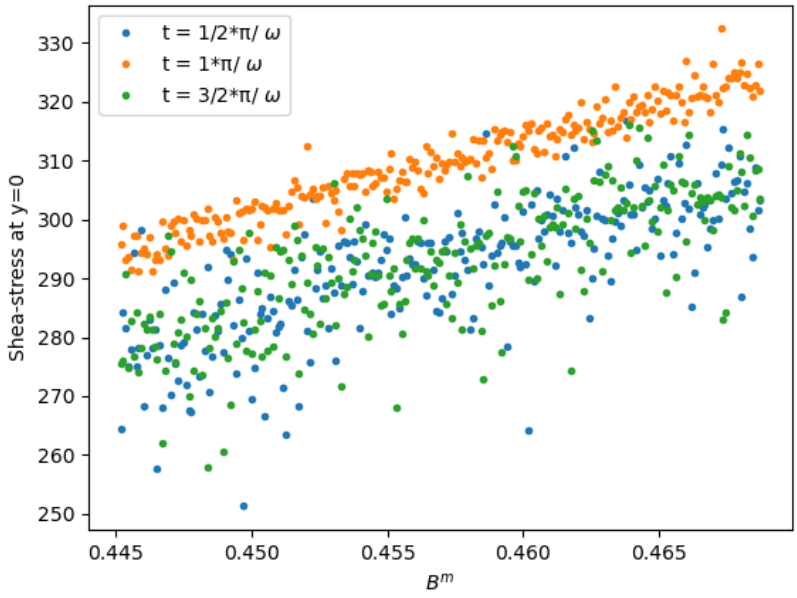

Figure 4.19.: The shear-stress against B^m of ketchup for $f = 3.7$ MHz at $k = 1$.

version of the code. It should be investigated why this plot is scattered in a future research. This could still be an instability in the step size in the z direction, but decreasing the step size significantly increases the computation time. It could also be caused by the amount of steps

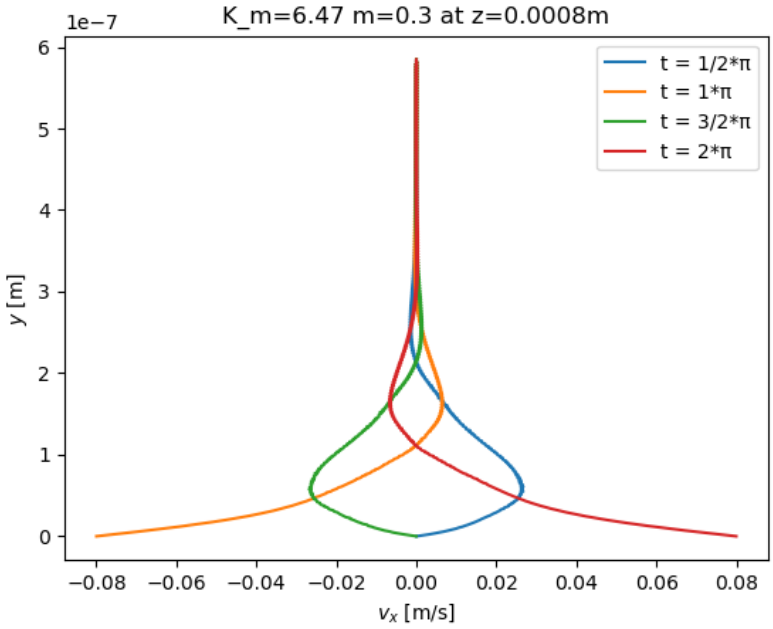

Figure 4.20.: The velocity profile of ketchup for $f = 3.7$ MHz at $k = 2$ for different time steps.

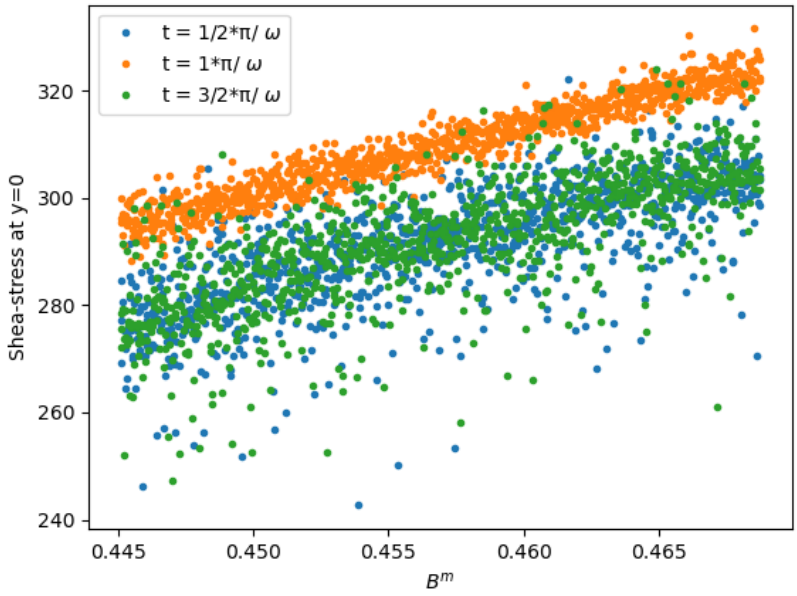

Figure 4.21.: The shear-stress against B^m of ketchup for $f = 3.7$ MHz at $k = 1$ with $\Delta z = 0.25 \cdot \lambda$.

in the z direction. Now only 0.2 m is examined in total with a small range of $B(z)$. To find a better relation it may be interesting to extend the plate and get a bigger range of $B(z)$ values to repeat this calculation with. Another cause for the instability could be the step size in the time

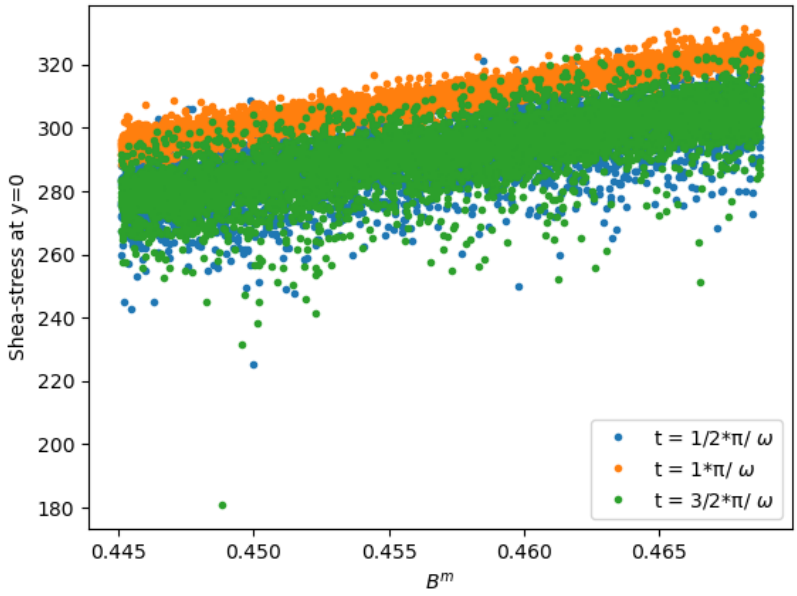

Figure 4.22.: The shear-stress against B^m of ketchup for $f = 3.7$ MHz at $k = 1$ with $\Delta z = \frac{\lambda}{20}$.

or the y direction. As the velocity profile seems stable the step size in the y direction seems good, thus looking at equation 3.18, it seems like the step size in the time could be decreased. It should be noted that in Figure 4.18 the shear-rate is much bigger compared to the other fluids. This also could be an indication to where the instability lies.

4.6. Blood

Because Ketchup is a shear-thinning fluid and the plot of the shear-stress against $B(z)^m$ was not usable another shear-thinning fluid was tested. This was blood, with $K_m = 9.267 \cdot 10^{-3}$ $[Pas^m]$, $m = 0.828$ and $\rho_f = 1060$ $[kgm^{-3}]$ as stated by [23]. First the amplitude attenuation was plotted. This is shown in Figure 4.23.

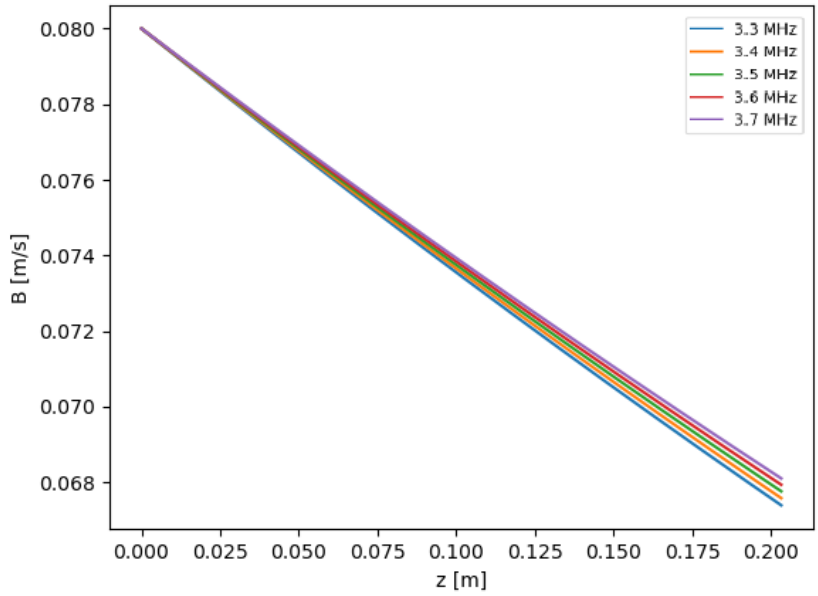

Figure 4.23.: The amplitude against the height of blood for different frequencies all with initial amplitude $B(0) = 0.08[m/s]$.

The attenuation is again not quite linear. Then the shear-stress was plotted against the shear-rate. The used frequency is again $f = 3.7$ MHz. This is shown in Figure 4.24. When the shape of Figure 4.24 is compared to Figure 2.2 it can be seen that is has indeed the shape of a shear-thinning fluid. Because of the value of m close to 1 it is closer to linear then the other shear-thinning fluids in this thesis.

The shear-stress was plotted against $B(z)^m$ and shown in Figure 4.25. When looking at this figure it can be seen that it approximated a linear relation quite well. Again a linear fit was applied and the root mean square errors calculated. The error for $t = 1/2 \cdot \pi/\omega$ is $\epsilon = 0.0192$ $[m/s]$, for $t = \pi/\omega$ the error is $\epsilon = 0.0197$ $[m/s]$ and for $t = 3/2 \cdot \pi/\omega$ the error is $\epsilon = 0.0195$ $[m/s]$. This is the fit that had the smallest root mean square error, and thus the fit that approximated a linear relation the best. Ethylene glycol approximated a linear relation the least.

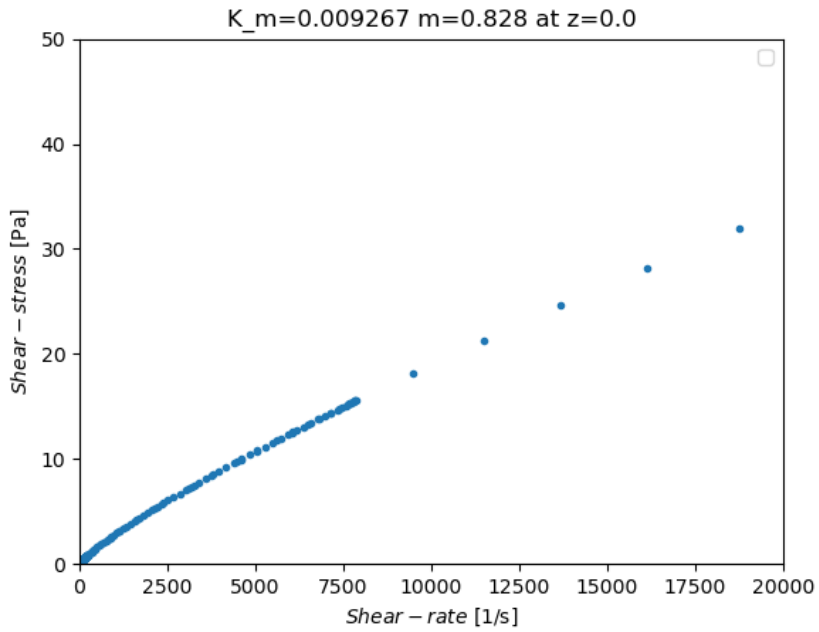

Figure 4.24.: The shear-stress against the shear-rate of blood for frequency $f = 3.7$ MHz at $k = 1$.

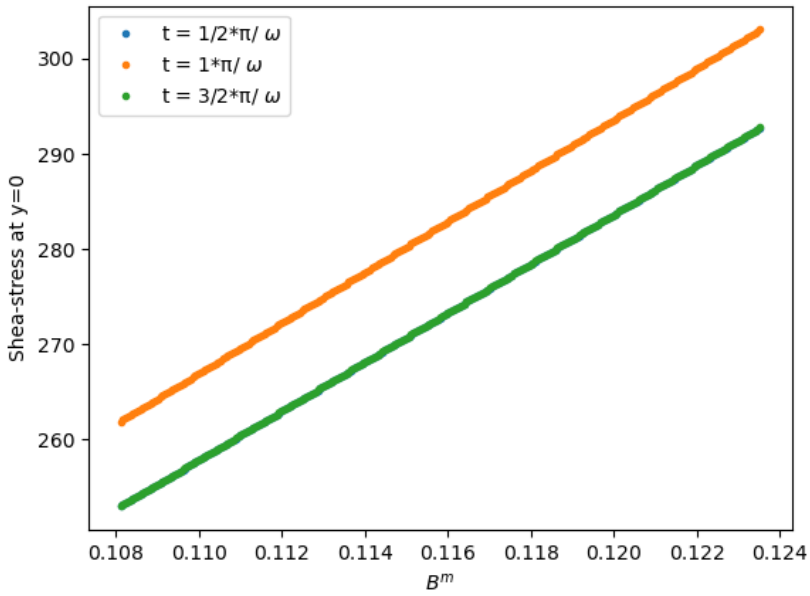

Figure 4.25.: The shear-stress against B^m of blood for $f = 3.7$ MHz at $k = 1$.

4.7. Comparing amplitude attenuation

Because most of the $\tau_{yx,0}$ against $B(z)^m$ graphs were almost linear it is interesting to so if there is much difference between the amplitude attenuation in this code versus in the previous version of the code. The proposed solutions only used that graph to determine K_m and m. So comparing those graphs can help give an insight in whether the assumption is valid. This will be done for ethylene glycol, blood and soybean oil as these fluids had an almost linear relation or linear relation when plotting shear-stress against $B(z)^m$. This is done by using the same amplitude and step size in the z direction with both codes.

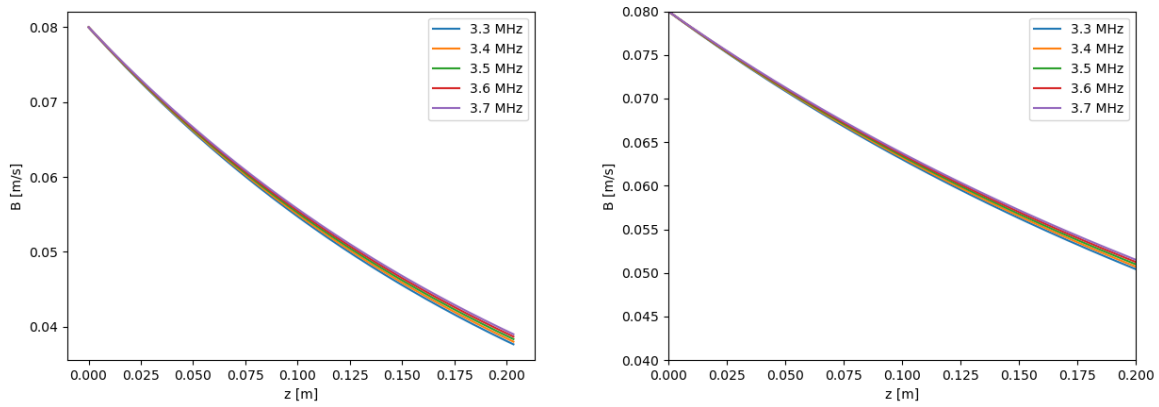

(a) The amplitude against the height for different frequencies all with the same initial amplitude simulated by the current version of the code.

(b) The amplitude against the height for different frequencies all with the same initial amplitude simulated by the previous version of the code.

Figure 4.26.: The amplitude attenuation at different frequencies with the same initial amplitude using two different versions of the code for ethylene glycol.

As can be seen in Figure 4.26 the left plot has a steeper decline in amplitude then the plot on the right. The plots are visibly different in slope.

This is repeated with soybean oil and the result is shown in Figure 4.27. In Figure 4.27 it can be clearly seen that again the attenuation is not the same. The slope of the current code is less steep then the slope of the previous version of the code. Lastly the same was done for blood. The result is shown in Figure 4.28.

In Figure 4.28 the difference in slope is less obvious. What is expected as the relation between the shear-stress and $B(z)^m$ approximated linear the best.

The two versions of the code do not produces the same attenuation plots and as the relation between the shear-stress and $B(z)^m$ was not linear, the approximation made is not valid.

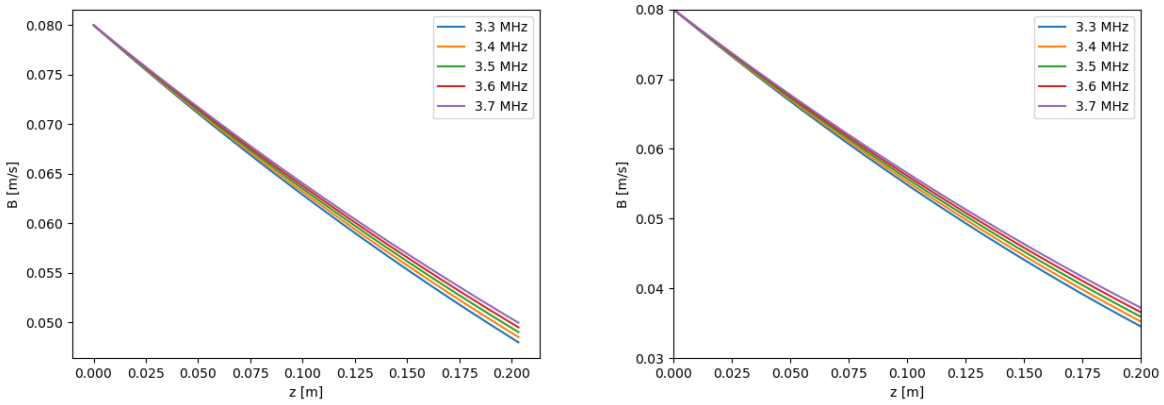

(a) The amplitude against the height for different frequencies all with the same initial amplitude simulated by the current version of the code.

(b) The amplitude against the height for different frequencies all with the same initial amplitude simulated by the previous version of the code.

Figure 4.27.: The amplitude attenuation at different frequencies with the same initial amplitude using two different versions of the code for soybean oil.

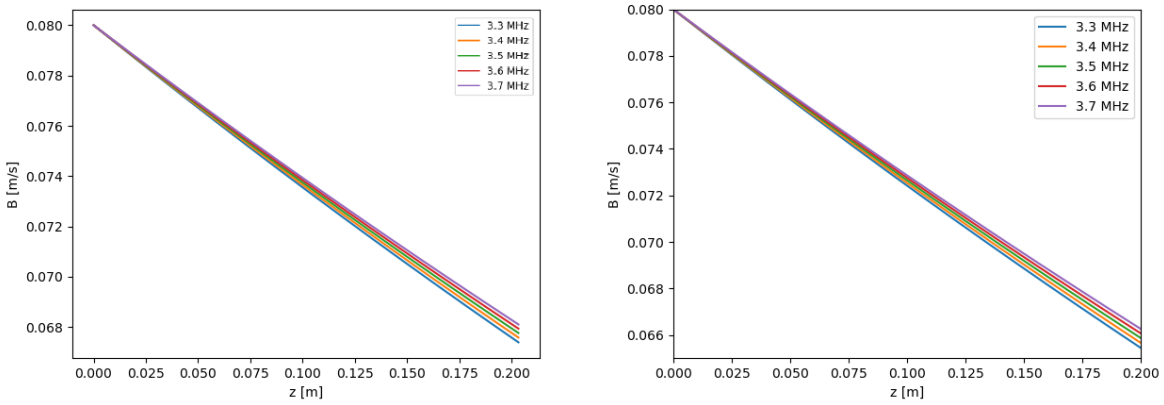

(a) The amplitude against the height for different frequencies all with the same initial amplitude simulated by the current version of the code.

(b) The amplitude against the height for different frequencies all with the same initial amplitude simulated by the previous version of the code.

Figure 4.28.: The amplitude attenuation at different frequencies with the same initial amplitude using two different versions of the code for blood.

Table 4.2.: The results of retrieving m and K_m using a linear fit compared to the literature values for three different fluids.

Fluid	m [-] literature	K_m $[Pas^m]$ literature	m [-] fit	K_m $[Pas^m]$ fit
Ketchup	0.3	6.47	0.7207	0.3074
Soybean oil	0.51	2.18	0.6757	2.8116
Ethylene glycol	1.29	0.0011	1.009	-0.0196

Table 4.3.: Values found for m and K_m by Borstlap [10] and Schuringa [11].

Fluid	m [-] Borstlap [10]	K_m $[Pas^m]$ Borstlap [10]	m [-] Schuringa [11]	K_m $[Pas^m]$ Schuringa [11]
Ketchup	0.2997	66.5368	0.2979	70.88
Soybean oil	0.5080	33.238	0.5093	33.32
Ethylene glycol	1.2943	7.8003e-7	1.289	9.271 e-7

4.7.1. Retrieving rheology

As the slopes in the amplitude attenuation plots are different for the two version of the code, it might be interesting to use the way of retrieving m and K_m that was used by Borstlap [10] and by Schuringa [11]. The results of the fit are shown in Table 4.2.

What can be seen in Table 4.2 is that the values of m and K_m are in the same order of magnitude as the literature values. The fitted value of K_m for ethylene glycol is non physical. It could be that the manner of fitting is not optimal and different manners of fitting should be investigated in future research. What should be noted is that a small range of z is used in this fit. The curve of the attenuation in not really visible, this makes finding the most accurate fit harder. The fit uncertainty will decrease when a bigger range of z is used for the fit. In future research this method of fitting could be applied to the simulation while using a bigger range of z to investigate the effect on the results.

When another initial amplitude was used for ethylene glycol, $B(z) = 0.8$ $[m/s]$, the fitted value for m stayed the same however the fitted value for K_m became $K_m = -0.03307$ $[Pas^m]$. It seems that the initial amplitude has influence on the retrieval of K_m and as in this thesis a much smaller initial amplitude is used than what both Borslap [10] and Schuringa [11] used, with about a factor 10^9, it should be investigated further what the exactly the effect of the initial amplitude is.

When comparing the results found with the current version of the code to the results found by Borstlap [10] and Schuringa [11], shown in Table 4.3, it should be noted that the values found by the current version of the code of m are further away from the literature values then with the version of the code used by Borstlap and Schuringa. However the values of K_m are much closer to the literature with this version of the code compared to the values found by Borstlap and Schuringa, except for the value of K_m for ethylene glycol which is not physical. Again note that in the current simulation a much smaller range of z was used than in the simulation of Borstlap and Schuringa.

In this thesis smaller, more realistic values are used for the length of the waveguide and amplitude. It seems to be more difficult to fit the parameters m and K_m for these more realistic constants.

5. Conclusion and recommendation

In this thesis a numerical simulation of the waveguide amplitude experiment has been made. An earlier version of a numerical simulation was checked to see if an assumption made to improve computation time was valid. By using this assumption it was no longer needed to calculate the rheology for every discrete z step. The code was rewritten to include the calculation of the rheology of every height. Then the code could be used to check the assumption.

This code was first benchmarked with water, as this has a known amplitude attenuation solution. When the experiment was simulated indeed an exponential relation between amplitude and height was found as expected from the theory. The influence of the step size in the height was investigated by simulating the experiment with different step sizes. There was a noticeable difference in the amplitude attenuation, but not in the velocity profile. To decrease computation time, $\Delta z = \lambda$ was used. The results of the simulation with a smaller step size could be explored.

For three different fluids the simulation was initially tested. These were soybean oil, ketchup and ethylene glycol. The shapes of the shear-stress against shear-rate plots match with the literature. For soybean and ethylene glycol it appeared that the relation between $\tau_{yx,0}$ and $B(z)^m$ was non linear, although it approximated a linear relation quite well. In the graph of ketchup a lot of scattering was visible. This could be a numerical instability and should be examined further. Lastly the relation was checked for blood. For this fluid the relation was linear. Because the relation between $\tau_{yx,0}$ and $B(z)^m$ was almost linear for soybean oil and ethylene glycol the amplitude attenuation was compared with the previous version of the code while using the same initial amplitude. When these were compared it was clear that the two codes produced an attenuation with different slopes. Finally m and K_m where retrieved and compared to the results of the previous versions of the code. Compared to the previous version m was less accurate, but still in the same order of magnitude. However, with the previous version of the code the values of K_m where not in the right order of magnitude. With the current version of the simulation they are in the right order of magnitude and thus much improved. The value of K_m found for ethylene glycol was negative and thus not physical. Other ways of finding m and K_m should be investigated to solve this problem. What should be noted is that only a small z range was simulated. This makes performing a fit more difficult. It is interesting to explore if the fit improves if the z range is increased.

The assumption made in the previous simulation is not valid as the relation between $\tau_{yx,0}$ and $B(z)^m$ for most fluids is not linear. It could be researched how much difference the two versions of the code make when the rheology is retrieved with other methods than used in this thesis, as the relations were really close to linear. If the difference is small, depending on the accuracy needed, the approximation could be used if reducing computation time plays a large role. Reducing the computation time could be investigated by reducing the amount of steps while still having numerical stability. Also the effect of the value of the initial amplitude should be researched as in previous research a much bigger amplitude was used than is this thesis. A different value K_m was found when the only changed parameter was the initial amplitude. Lastly the simulation could be extended to Bingham and Casson fluids as well.

Bibliography

[1] Molten salt reactors - world nuclear association. https://world-nuclear.org/information-library/current-and-future-generation/molten-salt-reactors.aspx.

[2] Project. https://samosafer.eu/project/, Oct 2019.

[3] Topics. https://www.martinrohde.nl/topics.html.

[4] W. P. Mason, W. O. Baker, H. J. Mcskimin, and J. H. Heiss. Measurement of shear elasticity and viscosity of liquids at ultrasonic frequencies. *Physical Review*, 75(6):936–946, 1949.

[5] T.K. Vogt, J.S. Lowe, and P. Cawley. Measurement of the material properties of viscous liquids using ultrasonic guided waves. *IEEE Transactions on Ultrasonics, Ferroelectrics and Frequency Control*, 51(6):737–747, 2004.

[6] Frederic Bert Cegla. *Ultrasonic waveguide sensors for fluid characterisation and remote sensing*. PhD thesis, 2006.

[7] M Rohde. Determining the rheology of power law fluids with a wave guide at high-frequency shear waves. Technical report.

[8] Remco Rook. Viscosity determination of newtonian fluids using shear ultrasonic guided wave attenuation, 2020.

[9] L. Ai and K. Vafai. An Investigation of Stokes' Second Problem for Non-Newtonian Fluids. *Numerical Heat Transfer, Part A: Applications*, 47(10):955–980, 2005.

[10] Lotte Borstlap. Numerical study on the determination of the rheological properties of power-law fluids in the ultrasonic waveguide experiment, 2020.

[11] Olivier Schuringa. Determination of rheological properties of power-law fluids using a numerical ultrasonic waveguide viscometer, 2021.

[12] Van Dijk, Sabine. Determining the shear-rate of shear-thinning fluids at the surface with an ultrasonic waveguide viscometer, 2021.

[13] Akker Harry van den and Rob Mudde. *Fysische Transportverschijnselen*. VSSD, 2008.

[14] F. Rizzo, F. Pinto, and M. Meo. Investigation of Silica-Based Shear Thickening Fluid in Enhancing Composite Impact Resistance. *Applied Composite Materials*, 27(3):209–229, 2020.

[15] Corina Fetecau, D. Vieru, and Constantin Fetecau. A note on the second problem of Stokes for Newtonian fluids. *International Journal of Non-Linear Mechanics*, 43(5):451–457, 2008.

[16] A Yew. Numerical differentiation: finite differences. https://www.dam.brown.edu/people/alcyew/apma0160.html, 2011.

[17] numpy.trapz - numpy v1.22 manual. https://numpy.org/doc/stable/reference/generated/numpy.trapz.html. Last accessed 14 june 2022.

[18] Nelson Moraga, Alejandra Torres, Abel Guarda, and María José Galotto. Non-Newtonian Canned Liquid Food, Unsteady Fluid Mechanics And Heat Transfer Prediction For Pasteurization And Sterilization. *Journal of Food Process Engineering*, 34(6):2000–2025, 2010.

[19] Vojtěch Kumbár, Sylvie Ondrušíková, and Šárka Nedomová. Rheological properties of tomato ketchup. *Potravinarstvo Slovak Journal of Food Sciences*, 13(1):730–734, 2019.

[20] Richard G. Green and Richard G. Griskey. Rheological Behavior of Dilatant (Shear-Thickening) Fluids. Part I. Experimental and Data. *Transactions of the Society of Rheology*, 12(1):13–25, 1968.

[21] Léon Peter Bernard Marie Janssen and Marinus Maria Cornelis Gerardus Warmoeskerken. *Transport phenomena data companion*. VSSD, 2006.

[22] numpy.polyfit — NumPy v1.23 Manual. https://numpy.org/doc/stable/reference/generated/numpy.polyfit.html.

[23] Sangho Kim, Young I. Cho, Abraham H. Jeon, Bill Hogenauer, and Kenneth R. Kensey. A new method for blood viscosity measurement. *Journal of Non-Newtonian Fluid Mechanics*, 94(1):47–56, 2000.

A. Energy loss derivation

Rohde [7] proposed the following derivation:

$$\Delta P_\tau = -2 \cdot \tau_0(z,t) \cdot v_x \cdot W \cdot dz \tag{A.1}$$

With $\tau_0(z,t)$ $[Pa]$ the shear-stress at the surface, V_x $[ms^{-1}]$ is the velocity of the shear-wave polarized in the x direction at the surface. There is a factor two because energy is lost at both sides of the waveguide. Energy loss at the bottom of the waveguide can be neglected because this area is much smaller. Also energy loss due to air can be neglected. Lastly internal friction will be neglected due to the elasticity of the waveguide [7].

The energy balance of the waveguide can be constructed. This results in the following:

$$h\frac{d}{dt}e_\omega(z,t) = -\frac{d}{dt}P'(z,t) - 2 \cdot \tau_0(z,t)v_x(y=0,z,t) \tag{A.2}$$

where P' $[Jm^{-1}s^{-1}]$is the power per unit length in the width direction that is transmitted in the z direction and e_ω $[Jm^{-3}]$ is the wave energy density [7].

This energy balance will now be time averaged. Due to the quasi-stationary condition:

$$\frac{1}{T}\int_T h\frac{d}{dt}e_\omega(z,t)dt = 0 \tag{A.3}$$

This leads the following time average of the spatial derivative:

$$\frac{1}{T}\int_T -\frac{d}{dz}P'(z,t)dt = -\frac{d}{dz}(\frac{1}{T}\int_T P'(z,t)dt) = -\frac{d}{dz}\tilde{P}'(z) \tag{A.4}$$

Which leaves the expression:

$$-\frac{d}{dz}\tilde{P}'(z) = -\frac{1}{T}\int_T 2 \cdot \tau_0(z,t)v_x(y=0,z,t)dt \tag{A.5}$$

with $\tilde{P}'(z) = \frac{1}{2}\rho_s h B(z)^2 c_s$ which leads to the final result:

$$B(z)\frac{dB(z)}{dz} = \frac{1}{\rho_s c_s h} \cdot \frac{1}{T}\int_T -2 \cdot \tau_0(z,t)v_x(y=o,z,t)dt \tag{A.6}$$

B. Step sizes

Schuringa [11] used the below explained step sizes and amount of steps, which where chosen so that there will not be numerical instability and the simulation will converge. How the used step sizes are calculated will be explained in this appendix. For Δt the following will be done:

$$T = 8/f \tag{B.1}$$

where T $[s]$ is the period and f $[1/s]$ is the frequency.

$$\Delta t = T/(Nt - 1) \tag{B.2}$$

with Nt the amount of time steps taken. In this thesis $Nt = 240001$.

For Δy first the maximum y value is determined. This is dependent on the skin depth, δ.

$$y_{end} = a \cdot (\frac{\omega \rho_f}{2K_m \omega^{m-1}})^{1/2} \tag{B.3}$$

where $a = 50$ for soybean oil, $a = 40$ for ketchup and blood and $a = 10$ for water and ethylene glycol.

After this Δy can be calculated.

$$\Delta y = \frac{y_{end}}{Ny - 1} \tag{B.4}$$

where Ny is the amount of steps taken in the y direction. In this thesis $Ny = 501$.